Geochemistry Geophysics Geosystems G3

Article
Volume 12, Number 12
7 December 2011
Q12004, doi:10.1029/2011GC003738
ISSN: 1525-2027

Published by AGU and the Geochemical Society

The nature of the crust beneath the Afar triple junction: Evidence from receiver functions

J. O. S. Hammond and J.-M. Kendall
School of Earth Sciences, University of Bristol, Wills Memorial Building, Queens Road, Bristol BS8 1RJ, UK (j.hammond@imperial.ac.uk)

G. W. Stuart
School of Earth and Environment, University of Leeds, Leeds LS2 9JT, UK

D. Keir
National Oceanography Centre Southampton, University of Southampton, Southampton SO14 3ZH, UK

C. Ebinger
Department of Earth and Environmental Sciences, University of Rochester, Rochester, New York 14627, USA

A. Ayele
Institute of Geophysics Space Science and Astronomy, Addis Ababa University, Addis Ababa, Ethiopia

M. Belachew
Department of Earth and Environmental Sciences, University of Rochester, Rochester, New York 14627, USA

Institute of Geophysics Space Science and Astronomy, Addis Ababa University, Addis Ababa, Ethiopia

[1] The Afar depression is an ideal locale to study the role of extension and magmatism as rifting progresses to seafloor spreading. Here we present receiver function results from new and legacy experiments. Crustal thickness ranges from ~45 km beneath the highlands to ~16 km beneath an incipient oceanic spreading center in northern Afar. The crust beneath Afar has a thickness of 20–26 km outside the currently active rift segments and thins northward. It is bounded by thick crust beneath the highlands of the western plateau (~40 km) and southeastern plateau (~35 km). The western plateau shows V_P/V_S ranging between 1.7–1.9, suggesting a mafic altered crust, likely associated with Cenozoic flood basalts, or current magmatism. The southeastern plateau shows V_P/V_S more typical of silicic continental crust (~1.78). For crustal thicknesses <26 km, high V_P/V_S (>2.0) can only be explained by significant amounts of magmatic intrusions in the lower crust. This suggests that melt emplacement plays an important role in late stage rifting, and melt in the lower crust likely feeds magmatic activity. The crust between the location of the Miocene Red Sea rift axis and the current rift axis is thinner (<22 km) with higher V_P/V_S (>2.0) than beneath the eastern part of Afar (>26 km, $V_P/V_S < 1.9$). This suggests that the eastern region contains less partial melt, has undergone less stretching/extension and has preserved a more continental crustal signature than west of the current rift axis. The Red Sea rift axis appears to have migrated eastward through time to accommodate the migration of the Afar triple junction.

Components: 2800 words, 11 figures, 3 tables.

Keywords: Ethiopia; receiver functions; rifting.

Index Terms: 8109 Tectonophysics: Continental tectonics: extensional (0905); 8137 Tectonophysics: Hotspots, large igneous provinces, and flood basalt volcanism; 8178 Tectonophysics: Tectonics and magmatism.

Received 9 June 2011; **Revised** 27 September 2011; **Accepted** 27 September 2011; **Published** 7 December 2011.

Hammond, J. O. S., J.-M. Kendall, G. W. Stuart, D. Keir, C. Ebinger, A. Ayele, and M. Belachew (2011), The nature of the crust beneath the Afar triple junction: Evidence from receiver functions, *Geochem. Geophys. Geosyst.*, *12*, Q12004, doi:10.1029/2011GC003738.

1. Introduction

[2] The Afar depression is a spectacular region that encompasses parts of Ethiopia, Eritrea and Djibouti (Figure 1). This harsh and sparsely populated area marks the intersection of the southern Red Sea rift (RSR), the Gulf of Aden rift (GOA) and the Main Ethiopian Rift (MER), forming an archetypal rift-rift-rift triple junction [*McKenzie et al.*, 1972; *Tesfaye et al.*, 2003]. The Afar sector is the most mature part of the East-Africa Rift system which divides the Nubian and Somalian plates along the MER, Nubian and Arabian plates along the RSR and Arabian and Somalian plates along the GOA [*Manighetti et al.*, 1998; *Beyene and Abdelsalam*, 2005].

[3] Recent active rifting and dike injection has focused scientific attention on this area [*Ebinger et al.*, 2010]. In September 2005, a 60 km long segment of the Dabbahu-Manda-Hararo (DMH) rift segment opened in two weeks [*Wright et al.*, 2006], and geodetic and seismic monitoring has revealed 14 episodes of dike injection along this segment of the rift [*Ayele et al.*, 2007; *Ebinger et al.*, 2008; *Ayele et al.*, 2009; *Keir et al.*, 2009a;*Hamling et al.*, 2009; *Grandin et al.*, 2010, 2011; *Belachew et al.*, 2011].

[4] An understanding of the crustal structure in the region provides insights into the thermal structure needed to understand passive margin development [e.g., *White and McKenzie*, 1989; *Buck*, 2004] and the processes involved with the transition from continental rifting to the formation of new oceanic crust. Here we use receiver functions (RF) to map variations in crustal structure and seismic properties that capture this transition in Afar, allowing us to test models of crustal modification by stretching and magma intrusion. We derive RFs from 49 broadband seismic stations, 41 of which are from the new Afar Consortium data set. On the periphery of Afar we include results of previous RF studies [*Dugda et al.*, 2005; *Dugda and Nyblade*, 2006; *Stuart et al.*, 2006]. Controlled source refraction experiments [e.g., *Berckhemer et al.*, 1975; *Makris et al.*, 1975; *Behle et al.*, 1975; *Egloff et al.*, 1991; *Mackenzie et al.*, 2005; *Maguire et al.*, 2006] provide additional control (Figure 1). We use a three stage approach, first constraining bulk crustal properties, second migrating the RFs to get a more complete 3D picture of crustal structure and finally waveform modeling of the RFs to constrain the internal crustal structure. Our results provide, for the first time, a comprehensive picture of crustal structure across the Afar depression, the youngest magmatic margin worldwide, and a first glimpse of the structure of incipient seafloor spreading.

2. Tectonic Setting

[5] The earliest rifting in this region occurred ~35 Ma in the Gulf of Aden [*d'Acremont et al.*, 2005], post-dating onset of volcanism on the Ethiopian plateau at ~40 Ma [*Davidson and Rex*, 1980; *Ebinger et al.*, 1993]. The highest eruption rates coincided with the onset of extension in the southern Red Sea in Afar [*Ukstins et al.*, 2002; *Wolfenden et al.*, 2005]. The volcanism associated with the inland Red Sea rift youngs to the south, and reached ~10°N ~10 Million years ago [*Wolfenden et al.*, 2004]. The third arm of the triple junction, the Main Ethiopian Rift, propagated northward from south Ethiopia ~18 Million years ago [*WoldeGabriel et al.*, 1990] and propagated into the Southern Red Sea rift at 10°N ~11 Million years ago [*Wolfenden et al.*, 2004]. Thus, no triple junction existed in this region until ~20 My after the emplacement of the flood basalts and the initial breakup forming the Red Sea and Gulf of Aden. As rifting commenced, Arabia moved north-eastward, resulting in the MER propagating north-eastward, cutting through older GOA (E-W) and RSR (NW-SE/N-S) trending structures [*Tesfaye et al.*, 2003; *Wolfenden et al.*, 2004; *Keir et al.*, 2011a]. The triple junction now lies in the vicinity of Lake Abhe on the Ethiopian/Djibouti border [*Tesfaye et al.*, 2003]. Oceanic crust is present in both the GOA [*d'Acremont et al.*, 2005] where it is thought

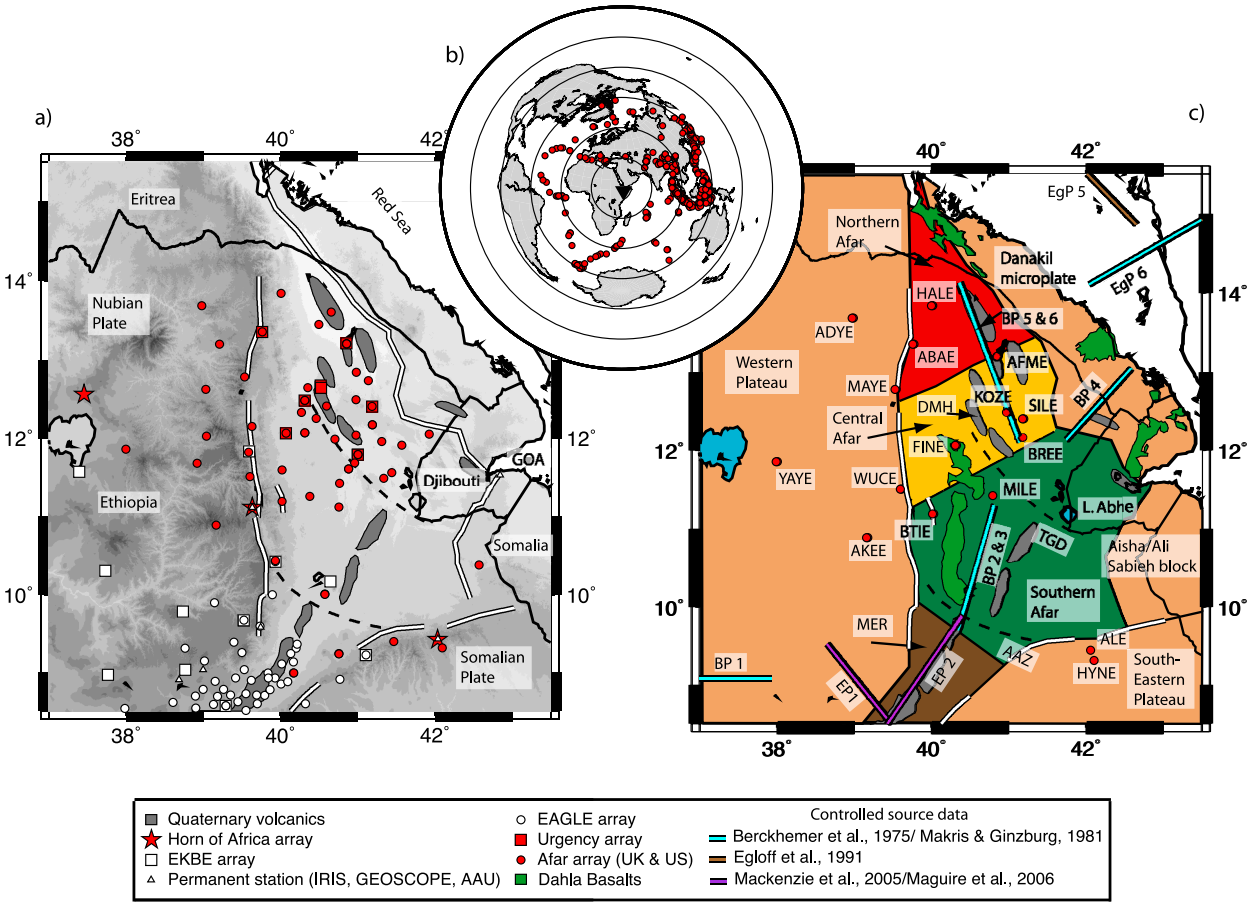

Figure 1. (a) Map showing the seismic stations in the Afar depression and surrounding region. Red stations show those used in this study, white stations show those where receiver functions have been generated in previous studies [*Dugda et al.*, 2005; *Dugda and Nyblade*, 2006; *Stuart et al.*, 2006; *Dugda et al.*, 2007]. See Key for details on different experiments. White lines demarcate the border faults, and dark grey shaded regions show regions of recent volcanism. (b) Map showing all the earthquakes used in this study. Inverted black triangle shows the location of the study area. (c) Map showing all places, stations and regions of the study area referred to in the text. BP, Berckhemer profiles; EP, EAGLE profiles; EgP, Egloff Profile; AAZ, Arcuate Accommodation Zone (southern dashed line); TGD, Tendaho-Gob'a Discontinuity (northern dashed line); DMH, Dabbahu-Manda-Hararo magmatic segment.

to extend into the Afar depression [*Manighetti et al.*, 1997], and at least as far south as 14°N in the Red Sea [*Prodehl et al.*, 1997]. At this latitude rifting is thought to migrate landward into the Afar depression [*Barberi et al.*, 1975; *Egloff et al.*, 1991; *Eagles et al.*, 2002]. Much of the deformation in Afar has now localized to ~60 km long, ~15 km wide axial volcanic ranges (magmatic segments) [*Hayward and Ebinger*, 1996].

[6] An added complexity in the Nubia/Somalia/Arabia breakup is the Danakil microplate (Figure 1), an area of highly stretched continental material [*Redfield et al.*, 2003], isolated due to the landward migration of Red Sea rifting between Arabia and Nubia. For approximately the last 3 Myr this microplate has rotated counter-clockwise independently of Arabia and Nubia [*Eagles et al.*, 2002], suggesting that the Danakil block will be isolated as the RSR and GOA rifts meet in Afar [*Eagles et al.*, 2002; *McClusky et al.*, 2010]. Continental material is also present in Djibouti and southern Afar in the form of the Ali Sabieh/Aisha block (Figure 1) [*Manighetti et al.*, 1998; *Audin et al.*, 2004; *Garfunkel and Beyth*, 2006]. The GOA rift seems to separate the Danakil from the Ali Sabieh/Aisha blocks, but the exact margins of these regions are poorly constrained.

3. Previous Studies of Crustal Structure in Ethiopia

[7] Three controlled source seismic experiments imaged down to uppermost mantle depths throughout

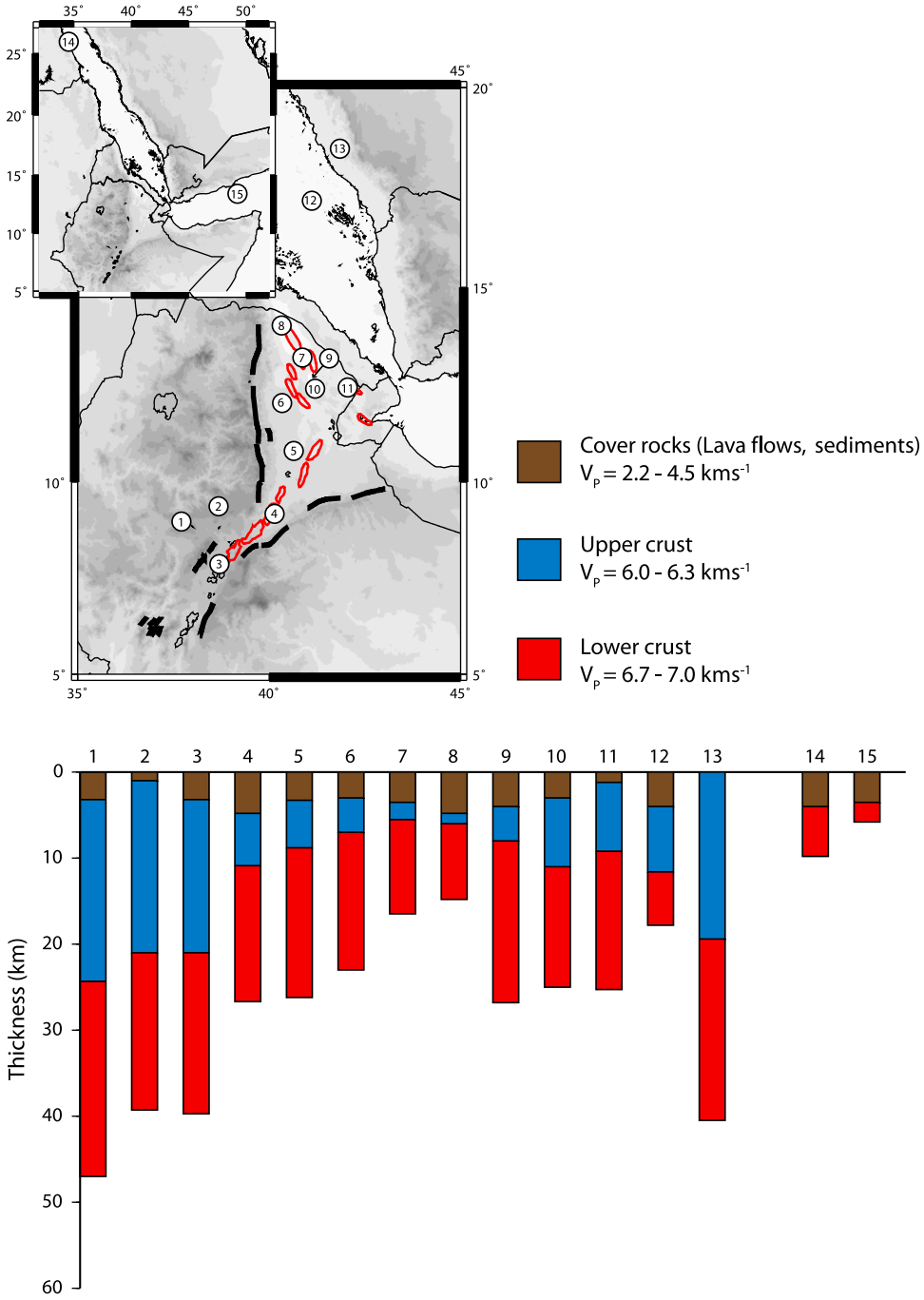

Figure 2. (top) Map showing the location of crustal sections. (bottom) A collection of crustal sections across the Afar Triple Junction region. The nomenclature is based on that of *Prodehl and Mechie* [1991]. Crustal sections are taken from *Laughton and Tramontini* [1969] (15), *Mechie et al.* [1986] (12,13), *Makris and Ginzburg* [1987] (2,5,8,9,11), *Gaulier et al.* [1988] (14), *Mackenzie et al.* [2005] (3,4), *Maguire et al.* [2006] (1) and this study (6,7,10).

our study area [*Berckhemer et al.*, 1975; *Makris and Ginzburg*, 1987; *Prodehl and Mechie*, 1991; *Mackenzie et al.*, 2005; *Maguire et al.*, 2006] (Figure 1). These studies show that the crust in Afar and the MER can be approximated by a three layer model (Figure 2). Following the nomenclature of *Prodehl and Mechie* [1991], this consists of a cover rock layer (e.g., sediments, volcanics) (*P*-wave velocity = 2.2–4.5 km s^{-1}), an upper crust (*P*-wave velocity = 6.0–6.3 km s^{-1}) and a lower crust (*P*-wave velocity = 6.7–7.0 km s^{-1}) above a

relatively low velocity mantle (*P*-wave velocity = 7.4–7.6 km s^{-1}).

[8] The cover rocks in this simple three layer model are up to 5 km thick in Afar (Berckhemer profile 4 and 5, Figure 1) [*Makris and Ginzburg*, 1987], and can include considerable evaporite deposits [*Behle et al.*, 1975]. Below this layer, the upper crust is interpreted by previous authors as Pan-African Precambrian crystalline basement in the MER and Afar, and as heavily intruded continental or incipient oceanic crust beneath magmatic segments [*Makris and Ginzburg*, 1987; *Mackenzie et al.*, 2005; *Maguire et al.*, 2006]. On the un-extended plateau the upper crust has a thickness of ~20–25 km [*Makris and Ginzburg*, 1987; *Mackenzie et al.*, 2005; *Maguire et al.*, 2006] (Figure 2). *Makris and Ginzburg* [1987] argue that, the thinned upper crust beneath Afar is not reflected in the lower crust, suggesting that the lower crust is thickened due to the emplacement of magmatic material. *Maguire et al.* [2006] suggest that the same applies for the MER, but acknowledge that to explain the uniform velocity seen in the lower crust from south to north, elevated temperatures must exist beneath the northern most extent of EAGLE profile 2 (Figure 1). *Makris and Ginzburg* [1987] show that the thinning upper crust and constant lower crust thickness continues from the northern MER into southern Afar, with upper crust thickness thinning from ~8 km in the south to ~4 km in the north whereas the lower crust has a constant thickness of ~18 km throughout (Figure 2). This pattern continues into central and northern Afar (herein referred to as Berckhemer profile 5 & 6, Figure 1), where upper crust thins from ~4 km in the south to almost non-existent in the north. Here, the lower crust also thins from ~16 km in the south to ~10 km in the north. *Bastow and Keir* [2011] theorize that the region of markedly thinned lower crust has resulted from stretching and thinning of the heavily intruded Afar crust, with an associated pulse of basaltic volcanism due to decompression melting in the underlying mantle. Thus the Precambrian crystalline basement may be present as the upper crust beneath a significant part of Afar. Complications to this model exist directly beneath volcanic segments, where elevated upper crustal velocities (*P*-wave velocity = 6.6 km s^{-1}) and increased density (300 kg m^{-3} density increase) are observed. These are interpreted as cooled intruded gabbroic bodies [*Keranen et al.*, 2004; *Mackenzie et al.*, 2005; *Cornwell et al.*, 2006]. Additionally, geochemistry of rocks from Afar magmatic segments show little evidence of crustal contamination [*Barrat et al.*, 2003], suggesting that the pre-Cambrian upper crust is absent at the <2Myr magmatic segments.

[9] Further evidence of crustal structure in the MER and surrounding plateau come from RF studies which provide estimates of crustal thickness and bulk crustal seismic properties [*Hebert and Langston*, 1985; *Dugda et al.*, 2005; *Stuart et al.*, 2006], as well as more detailed images of internal crustal structure [*Dugda and Nyblade*, 2006; *Dugda et al.*, 2007; *Cornwell et al.*, 2010]. These show crustal thicknesses comparable to the controlled source results, but also provide information on the ratio of *P*-wave velocity to *S*-wave (hereafter referred to as V_P/V_S).

[10] Previous RF studies south of our study area [*Dugda et al.*, 2005; *Stuart et al.*, 2006; *Dugda and Nyblade*, 2006; *Dugda et al.*, 2007; *Cornwell et al.*, 2010] show that the crust beneath the MER has extremely high V_P/V_S (>2), beneath the western plateau it has high V_P/V_S (1.8–1.9) and the south-eastern plateau shows typical continental rock type values (<1.8) [*Christensen*, 1996]. These values are averages for the whole crust, thus high V_P/V_S values above ~1.9 likely indicate the presence of fluid, most likely partial melt throughout a large part of the crust. This, along with the presence of recent seismicity [*Keir et al.*, 2006], highly conductive bodies [*Whaler and Hautot*, 2006], Quaternary eruptive centers [*Hayward and Ebinger*, 1996] and numerous hotsprings points toward ongoing magmatism underlying the recent Quaternary magmatic segments in the center of the MER. Additionally, studies of crustal and mantle anisotropy suggest that magma input into the crust increases northward through the MER toward Afar [*Ayele et al.*, 2004; *Kendall et al.*, 2005; *Bastow et al.*, 2010; *Keir et al.*, 2011b].

4. Data and Methodology

[11] We use data from temporary seismic deployments in the Afar depression and surrounding plateau (Figure 1). The main new data set comes from the multinational collaborative Afar Consortium project (UK, US and Ethiopia); a SEIS-UK and IRIS-PASSCAL deployment of 41 stations throughout the Afar region. These include 3 CMG-3T (120 s natural period), 23 CMG-ESP (60 s natural period), 14 CMG-40T (30 s natural period) and 1 CMG-6TD (30 s natural period) Guralp seismometers. Stations were deployed from March 2007 to October 2009 after which the array was condensed to 12 CMG-ESP sensors, which are still

recording (September 2011) ongoing seismic and volcanic activity. Additionally, we use data from 9 CMG-6TD sensors deployed in response to the September 2005 dike injection at DMH (Urgency Array) [*Ebinger et al.*, 2008; *Keir et al.*, 2009a; *Ebinger et al.*, 2010], which recorded from October 2005 to February 2007 and 3 RLBM (Réseau Large Bande Mobile) stations deployed as part of the French 'Horn of Africa' project, which ran from June 1999 to December 2002 [*Sebai et al.*, 2006]. Station locations can be found in Figure 1 and details in Table 1. All data were continuous and recorded with a sample rate of 50 Hz, except the RLBM data which were recorded with a sample rate of 20 Hz.

[12] To image crustal structure beneath Afar we use the receiver function (RF) technique [*Langston*, 1979], which removes *P*-wave energy from teleseismic seismograms using deconvolution, thus enhancing *S*-wave energy converted at boundaries in the crust and upper mantle. We use the extended-time multitaper RF technique of *Helffrich* [2006], which, by using multitaper analysis in the deconvolution step [*Park and Levin*, 2000], allows for generation of broad-band RFs of arbitrary length.

[13] To construct RFs we use teleseismic earthquakes (mb > 5.5) from distances of 30°–90° to eliminate the effects of upper mantle triplications and core phases. This results in 404 earthquakes (290–Afar Consortium array, 38–Urgency array, 76–RLBM array), of sufficient signal to noise level to provide quality RFs (Figure 1). A frequency domain low-pass $\cos^2$ taper with a 1.5 Hz low-pass cut-off frequency is applied to the RFs. In general the data quality is high due to absence of cultural noise, resulting in a total of 3914 RFs (Table 1).

[14] Figure 3 shows RF stacks from a selection of stations across the Afar depression and the surrounding highlands. Stacks are calculated using a jackknife averaging approach [*Efron*, 1982]. This involves removing one trace at a time from the data, and calculating a sum of the subset of data. This is repeated $n - 1$ times, where n is the number of receiver functions. The average of these stacks provides the estimated jackknife stack and the standard deviation of all the stacks provides an estimate of the error of the stacked receiver function.

[15] The RFs, based on their waveform characteristics, can be split into 4 groups: (1) western plateau, (2) southeastern plateau, (3) southern/central Afar and (4) northern Afar. RFs on the western and southeastern plateaus show a clear Moho Ps conversion at 4–6 s and positive and negative peaks at 15–25 s associated with reverberations in the crust (Figure 3). Southern and central Afar stations show clear Moho Ps conversions between 3 and 5 s and multiples between 10 and 20 s. Northern Afar stations show Moho Ps arrivals occur between 1 and 3 s with multiples between 6 and 13 s.

5. H-κ Stacking

[16] The first stage in our three step approach is obtaining an estimate of the bulk crustal structure across Afar using the H-κ stacking technique [*Zandt and Ammon*, 1995; *Zhu and Kanamori*, 2000]. This enables us to estimate the crustal thickness (H), and bulk crust V_P/V_S (κ).

[17] For a given slowness of incoming *P*-wave, the arrival time of a *P*-*S* conversion (relative to the *P*-wave arrival), and also the arrival times of conversions which reverberate once in a layer beneath a station can be calculated (see *Zhu and Kanamori* [2000] for details). The arrival time of these conversions depends on the thickness of the layer (H), and V_P/V_S (κ), assuming an average *P*-wave velocity for the crust. In our case we are fortunate that we have an estimate of *P*-wave velocities from nearby legacy refraction profiles [e.g., *Makris and Ginzburg*, 1987; *Mackenzie et al.*, 2005] (Table 1). Average V_P values for the western and southeastern plateaus are taken as 6.25 km s^{-1} and for Afar between 6.15 km s^{-1} and 6.25 km s^{-1} (see Table 1 for details). These average crustal velocities are the same as those used by *Stuart et al.* [2006]; we find that the average crustal velocity assumed by *Dugda et al.* [2005] slightly high (6.5 km s^{-1}) meaning their results may over-estimate crustal thickness. In this study we are concentrating on the crustal structure in Afar and the surrounding region. Where our new Afar network stations are co-located with stations from previous studies (TEND/SEME, DIYA/WLDE, MISE/MIEE, KORE/KARA/KARE), we reanalyzed all RFs and H-κ stacking was performed using the average crustal V_P in Table 1. A grid search is performed over plausible values of H and κ, calculating the theoretical arrival time for *Ps* (the conversion from a *P*-wave to an *S*-wave at the Moho), *PpPs* (energy that reverberate once in a layer, converting to an *S*-wave at the last bounce point), and PpSs or PsPs (reverberations which convert to an *S*-wave at an earlier bounce point, thus arriving later). These values are calculated for each individual RF, thus accounting for slowness. The RF amplitude at the theoretical times for the primary (*Ps*) and multiples (*PpPs*, *PsPs*/*PpSs*) are summed (all phases are weighted equally), and the sum will

Table 1. H-κ Stacking Results for Afar Stations[a]

Station	Experiment	Longitude	Latitude	H (km)	$Error_B$ (km)	$Error_{V_P}$ (km)	κ	$Error_B$	$Error_{V_P}$	V_P (km s^{-1})	RFs
				Western Plateau							
ABAE WEST	AFAR	39.35	13.35	**32**	**6**	1	**1.82**	**0.20**	0.02	6.25	14
ADYE	AFAR	38.98	13.68	**39**	0	**1**	**1.71**	**0.02**	0.01	6.25	85
AKEE	AFAR	39.16	10.88	**38**	**4**	2	**1.91**	**0.06**	0.01	6.25	50
DERE/DSS	AFAR/RLBM	39.64	11.12	**32**	**4**	1	**2.01**	**0.12**	0.01	6.25	90
GASE	AFAR	38.92	11.68	**43**	**6**	2	**1.85**	**0.11**	0.01	6.25	18
GDR	RLBM	37.45	12.56	**39**	**5**	2	**1.83**	**0.15**	0.02	6.25	7
KORE	AFAR										
KARE	EAGLE	39.93	10.44	**45**	**2**	2	**1.78**	**0.05**	0.01	6.25	49
KARA	EKBE										
LALE[b]	AFAR	39.04	12.02	**38**			**1.85**			6.25	30
SEKE	AFAR	39.03	12.62	**38**	**2**	2	**1.81**	**0.07**	0.03	6.25	44
SMRE	AFAR	39.21	13.19	**39**	**2**	2	**1.77**	**0.07**	0.01	6.25	72
WLDE	AFAR										
DIYA	EKBE	39.59	11.82	**37**	**4**	2	**1.72**	**0.10**	0.03	6.25	15
WUCE WEST	AFAR	39.19	11.51	**33**	**7**	1	**1.89**	**0.17**	0.01	6.25	9
YAYE[b]	AFAR	38.00	11.86	**44**			**1.86**			6.25	6
				Southeastern Plateau							
ALE	RLBM	42.03	09.42	**35**	**1**	1	**1.79**	**0.07**	0.01	6.25	28
HYNE	AFAR	42.09	09.31	**35**	0	**1**	**1.77**	**0.01**	0.00	6.25	81
				Southern Afar							
BOBE	AFAR	42.57	10.38	**27**	**3**	1	**1.77**	**0.16**	0.02	6.25	37
MISE	AFAR										
MIEE	EAGLE	40.76	09.24	**32**	**5**	2	**2.22**	**0.28**	0.02	6.25	41
QATE	AFAR	41.47	09.40	**32**	**6**	1	**2.27**	**0.21**	0.02	6.25	67
				Central Afar							
ASYE	AFAR	41.44	11.56	**28**	**5**	1	**1.95**	**0.14**	0.01	6.25	107
AWEE	AFAR	40.07	12.06	**25**	**1**	1	**1.83**	**0.04**	0.04	6.15	78
BREE	AFAR	41.19	12.17	**26**	**1**	1	**1.84**	**0.02**	0.01	6.15	95
BTIE EAST	AFAR	40.29	11.19	**23**	**3**	1	**2.20**	**0.14**	0.01	6.25	126
CHIE	AFAR	40.02	11.60	**28**	**3**	1	**1.84**	**0.11**	0.02	6.25	105
DAME[b]	AFAR	40.96	11.69	**31**			**1.97**			6.15	23
DICE	AFAR	41.57	11.91	**30**	**5**	1	**2.02**	**0.20**	0.01	6.15	47
DIGE	AFAR	40.27	12.32	**17**	**1**	1	**2.26**	**0.06**	0.01	6.15	66
ELLE	AFAR	40.37	11.25	**27**	**7**	1	**2.07**	**0.22**	0.01	6.15	45
FINE	AFAR	40.31	12.06	**22**	0	**1**	**1.99**	**0.03**	0.02	6.15	154
HARE	AFAR	40.88	11.60	**25**	**1**	1	**1.99**	**0.04**	0.03	6.15	45
IGRE	AFAR	40.46	12.25	**23**	**5**	1	**1.85**	**0.20**	0.02	6.25	45
KOBE	AFAR	39.63	12.15	**29**	0	**1**	**1.84**	**0.02**	0.01	6.25	52
KOZE	AFAR	40.98	12.49	**28**	**2**	1	**1.84**	**0.07**	0.02	6.15	46
LULE	AFAR	40.70	11.99	**24**	**2**	1	**1.98**	**0.07**	0.02	6.15	39
LYDE	AFAR	41.92	12.05	**29**	**2**	1	**2.19**	**0.11**	0.02	6.15	30
MAYE EAST	AFAR	39.77	12.78	**21**	0	**1**	**1.93**	**0.03**	0.02	6.25	80
MILE	AFAR	40.77	11.42	**33**	**5**	1	**1.88**	**0.11**	0.02	6.15	42
SEHE	AFAR	40.97	12.04	**22**	0	**1**	**1.98**	**0.02**	0.02	6.15	146
SEME	AFAR										
TEND	EKBE	41.00	11.79	**25**	**5**	1	**2.02**	**0.15**	0.03	6.15	114
SILE	AFAR	41.18	12.40	**24**	**1**	1	**2.00**	**0.03**	0.01	6.15	66
SRDE	AFAR	41.30	11.95	**24**	**3**	1	**2.04**	**0.12**	0.01	6.15	32
TRUE	AFAR	40.31	12.48	**23**	**1**	1	**1.97**	**0.03**	0.01	6.15	115
WUCE EAST	AFAR	39.92	11.51	**26**	**8**	1	**2.11**	**0.25**	0.02	6.25	59
				Northern Afar							
ABAE EAST	AFAR	39.98	13.35	**19**	0	**1**	**2.09**	0.04	**0.05**	6.25	93
AFME	AFAR	40.85	13.20	**16**	0	**1**	**2.06**	0.01	**0.02**	6.25	161
HALE	AFAR	40.01	13.84	**20**	**2**	1	**1.98**	**0.10**	0.04	6.15	17

[a] $Error_B$ shows the bootstrap determined error estimate and $Error_{V_P}$ shows the error estimate based on a sensitivity test of the assumed average V_P. The bolded results were used in this study.

[b] V_P/V_S are estimated from nearby stations as no clear multiples are observed.

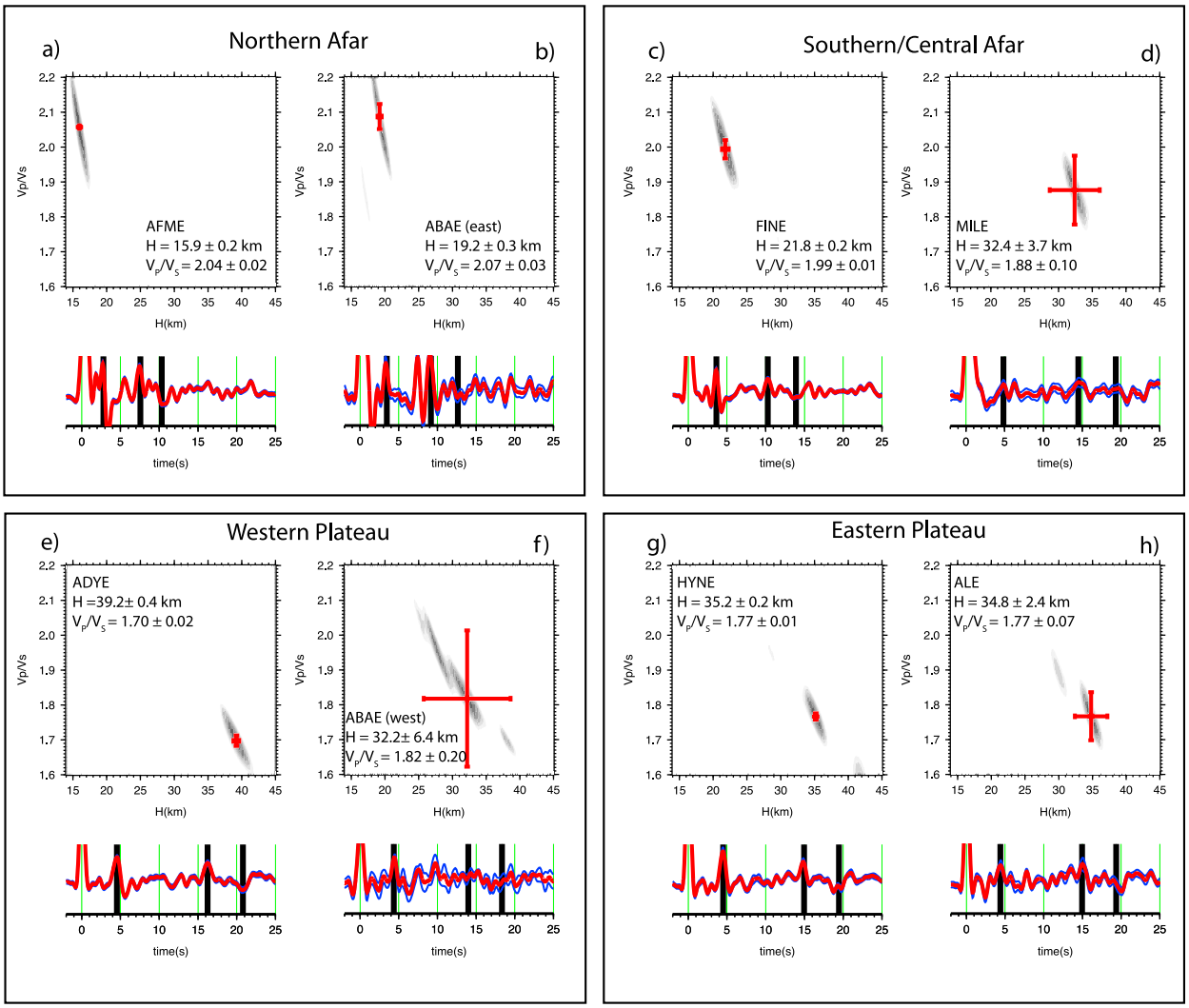

Figure 3. H-κ estimates of crustal thickness for (a) AFME, (b) ABAE (events with eastern back-azimuths only), (c) FINE, (d) MILE, (e) ADYE, (f) ABAE (events with western back-azimuths only), (g) HYNE and (h) ALE. For each plot the top panel shows the H-κ stacked result, with the red cross showing the best result, with associated bootstrap error bars. The bottom panel shows the stacked receiver function where the black receiver function is the jackknife stack, and the blue receiver functions show the 1σ jackknife errors. The black lines show the theoretical arrival times for the *Ps*, *PpPs* and *PsPs*/*PpSs* phases for an event from distance 65° and based on the best estimate of H and κ.

be largest when the optimum values of H and κ are used [*Zhu and Kanamori*, 2000] (Figure 3). Typically the discontinuity is the Moho, and this signal dominates the RF giving the largest amplitude in the H-κ domain. Errors are calculated using two methods; a bootstrap method [*Efron and Tibshirani*, 1991] and a sensitivity test based on possible errors in the assumed average crustal V_P. To estimate the bootstrap error we randomly choose RFs from the data set (it is possible for a receiver function to be included more than once) and estimate H and κ from a new set of RFs (keeping the number of RFs the same as that used in the original data set). This procedure is repeated 10,000 times, and the standard deviation of these 10,000 results is our estimate of error. Bootstrap error estimates give a good idea of the stability of our result. Another source of error is in the assumed value of V_P. We have better constraints on this due to nearby controlled source profiles, however *Mackenzie et al.* [2005] estimate that errors in the velocity values can be 0.2 km s^{-1}. As a result we recalculate the H-κ result with the assumed V_P value ±0.2 km s^{-1}, and use the range of H-κ estimates as another estimate of error. Whichever is largest is the value we use in this study (Table 1).

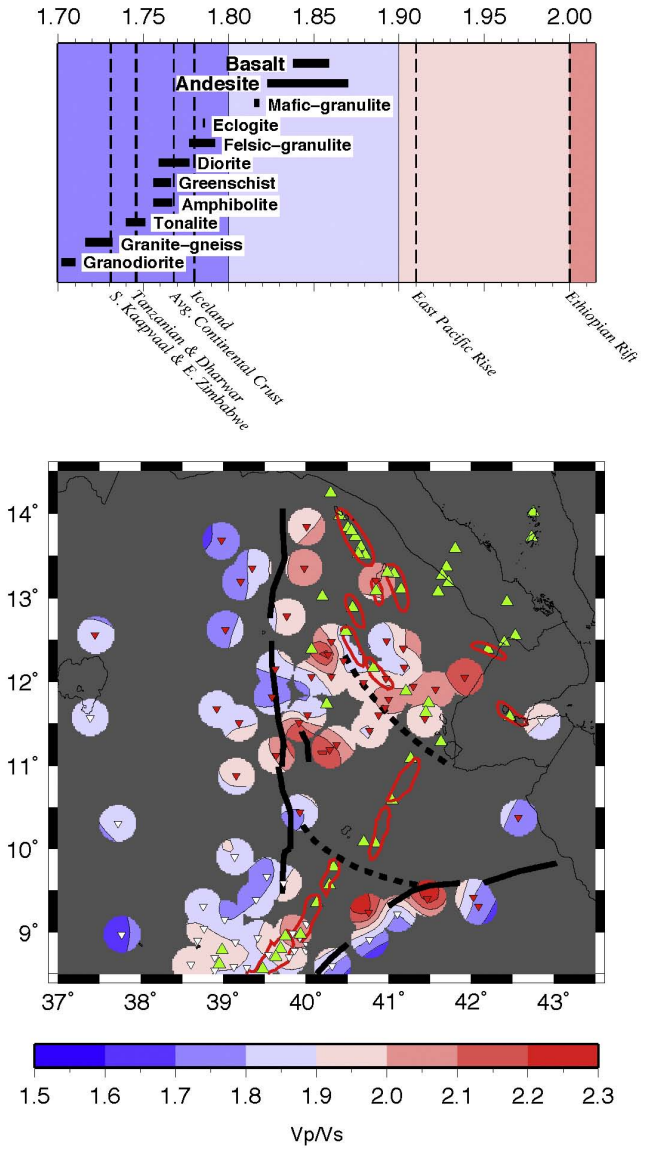

Figure 4. (top) Typical V_P/V_S for common crustal lithologies [*Christensen*, 1996], adapted from *Thompson et al.* [2010]. See *Thompson et al.* [2010] for references to V_P/V_S for different regions, except East Pacific Rise which is taken from *Harmon et al.* [2007]. (bottom) A map of V_P/V_S based on receiver function results from this and previous receiver function studies [*Dugda et al.*, 2005; *Dugda and Nyblade*, 2006; *Stuart et al.*, 2006]. Inverted triangles indicate the location of receiver function V_P/V_S estimates (red, this study; white, previous studies). Green triangles show the location of active volcanoes [*Siebert and Simkin*, 2002]. Black lines show the border faults separating Afar from the western and southeastern plateaus. The dashed line shows the Tendahao-Gob'a discontinuity (northern line) and arcuate accommodation zone [*Tesfaye et al.*, 2003] (southern line). The red lines demarcate the quaternary volcanic segments. Regions shaded grey mask regions with no data coverage.

[18] Figure 3 and Table 1 show a selection of H-κ results for the southeastern and western plateaus and south, central and northern Afar. Typically, a Ps conversion occurs almost directly beneath a station (within 6 km for an event from 65° distance arriving at a Moho 26 km deep). However, multiples will be sensitive to a much wider region (within 26 km for an event from 65° distance arriving at a Moho 26 km deep). To account for this the results shown in Figures 4 and 5 highlight areas within 25 km of a station. Some stations (ABAE, BTIE, MAYE, WUCE, see Figure 1 for station locations) have strongly varying Ps arrivals that are dependent on back-azimuth (e.g., ABAE

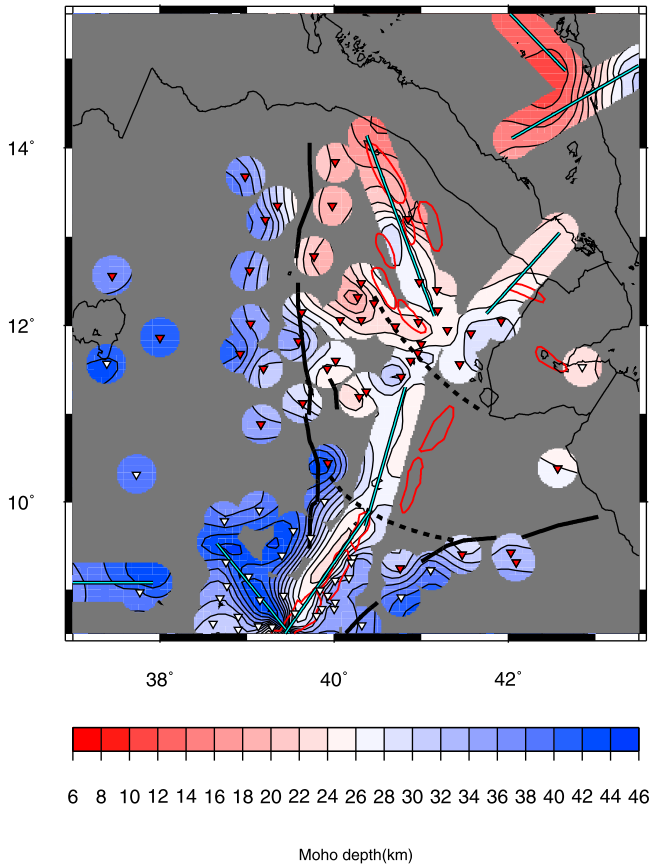

Figure 5. A map of Moho depth based on receiver function results from this and previous receiver function studies [*Dugda et al.*, 2005; *Dugda and Nyblade*, 2006; *Stuart et al.*, 2006] and controlled source work [*Berckhemer et al.*, 1975; *Makris and Ginzburg*, 1987; *Egloff et al.*, 1991; *Mackenzie et al.*, 2005; *Maguire et al.*, 2006]. Triangles indicate the location of receiver function Moho depth estimates (red, this study, white, previous studies), and the cyan lines show the location of controlled source Moho depth estimates. Black lines show the border faults separating Afar from the western and southeastern plateaus. The dashed line shows the Tendahao-Gob'a discontinuity (northern line) and arcuate accommodation zone [*Tesfaye et al.*, 2003] (southern line). The red lines demarcate the quaternary volcanic segments. Regions shaded grey mask regions with no data coverage.

lies at the boundary between the western plateau and northern Afar, Figure 1). In these cases H-κ stacking is performed on events from selected back-azimuths, similar to the study of *Dugda et al.* [2005] for stations in southern Afar. In these cases, the results plotted in Figures 4 and 5 are shown at the first Moho bounce point of the PpPs multiple for the dominant back azimuth.

[19] Figures 4 and 5 show contour maps of the Moho depth and bulk crust V_P/V_S (Table 1) from the H-κ technique. Included with the results from our new Afar network are estimates from previous RF studies [*Dugda et al.*, 2005; *Dugda and Nyblade*, 2006; *Stuart et al.*, 2006], as well as estimates of crustal thickness from controlled source experiments [*Makris and Ginzburg*, 1987; *Egloff et al.*, 1991; *Mackenzie et al.*, 2005]. To compare different studies we plot all Moho depths with respect to sea level. Figure 6 shows a comparison of estimates of Moho depth from refraction experiments and RF studies (where seismic stations are within 15 km of the refraction profile). The RF results tend to be shallower than the refraction estimates, possibly due to the fact that refraction estimates are based on rays diving below the discontinuity. However, some large discrepancies do exist. A notable difference occurs in regions where lower crustal high velocity layers, interpreted as intrusives related to Cenozoic flood basalt volcanism, have been imaged on the southwestern plateau [*Mackenzie et al.*, 2005; *Maguire et al.*, 2006; *Cornwell et al.*, 2010]. As a result, the RF and refraction studies may be imaging different layers (as also suggested by *Stuart et al.* [2006]). Refraction studies and RFs show a rapidly thinning

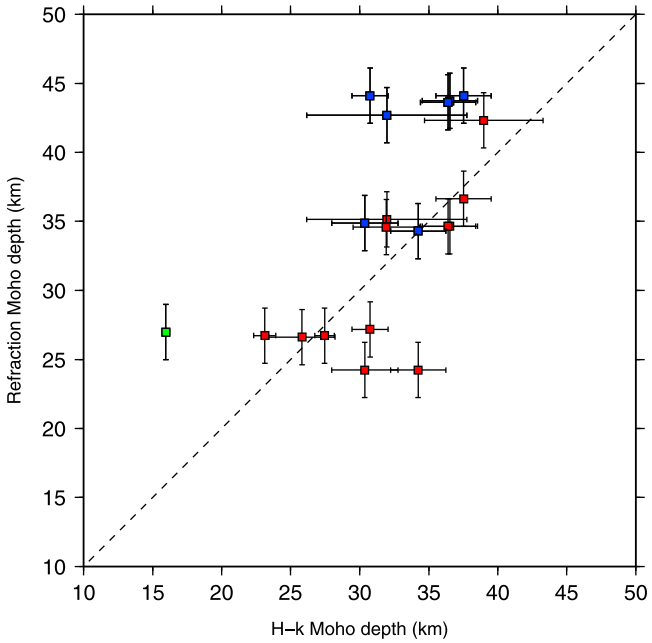

Figure 6. A comparison of refraction study estimates of Moho depth [*Berckhemer et al.*, 1975; *Makris and Ginzburg*, 1987; *Mackenzie et al.*, 2005; *Maguire et al.*, 2006] and receiver function estimates of Moho depth [*Dugda et al.*, 2005; *Dugda and Nyblade*, 2006; *Stuart et al.*, 2006; this study]. Blue symbols relate to EAGLE profile 1 (see Figure 1), where the presence of a lower crustal high velocity layer is present. The green symbol relates to station AFME, which is located above a sharp change in crustal thickness [*Berckhemer et al.*, 1975; *Makris and Ginzburg*, 1987].

crust (26 km to 16 km over ~100 km [*Makris and Ginzburg*, 1987]). However, the RFs, which have much larger Fresnel zones than the refraction study, may estimate thinner crust at a point close to this transition compared to the high frequency controlled source data. However, these differences aside, the refraction studies and the RF studies agree reasonably well, suggesting that the Moho and V_P/V_S maps can be interpreted with confidence.

5.1. Western and Southeastern Plateaus

[20] On the western plateau the crustal thickness ranges from 32 ± 4 km to 45 ± 2 km. Controlled source, and previous RF work, have shown evidence for lower crustal high velocity layers [*Mackenzie et al.*, 2005; *Maguire et al.*, 2006; *Cornwell et al.*, 2010], which are interpreted as highly intruded lower crust. This may explain the large range of crustal thickness as these two layers may dominate the RF at different stations. As further support, the two stations on the SE plateau where flood basalts are thin (<500 m) and younger than along the western plateau [e.g., *Wolfenden et al.*, 2004] show consistent results (35 ± 1 km) (Table 1 and Figure 5), although more stations are needed to fully constrain this.

[21] The ratio of *P*-wave velocity to *S*-wave velocity (V_P/V_S), also shows much variation between the southeastern and western plateaus. In general the western plateau shows V_P/V_S of 1.7–1.9, with stations south of ~11.5°N having V_P/V_S of 1.8–1.85 (Figure 4), whereas north of ~11.5°N the V_P/V_S is typically below 1.80. The southern part of the western plateau V_P/V_S are higher than average values for continental crust (1.77 [*Christensen*, 1996]), and indicate continental crust is more mafic, most probably associated with intrusives of the Cenozoic flood basalts (Figure 4). Also, ongoing magmatism and partial melt in the lower crust, as suggested by magneto-telluric studies [*Whaler and Hautot*, 2006], seismic anisotropy [*Kendall et al.*, 2005; *Bastow et al.*, 2010; *Hammond et al.*, 2010], and seismicity [*Keir et al.*, 2009b] will increase the average crustal V_P/V_S. The southeastern plateau and the northern part of the western plateau, which are not covered by flood basalts, show V_P/V_S more typical of continental crust (1.79 ± 0.07, 1.77 ± 0.01). The asymmetry between southeastern and western plateaus supports previous work that suggests an inherent difference in structure beneath the two [see *Bastow et al.*, 2011, and references within].

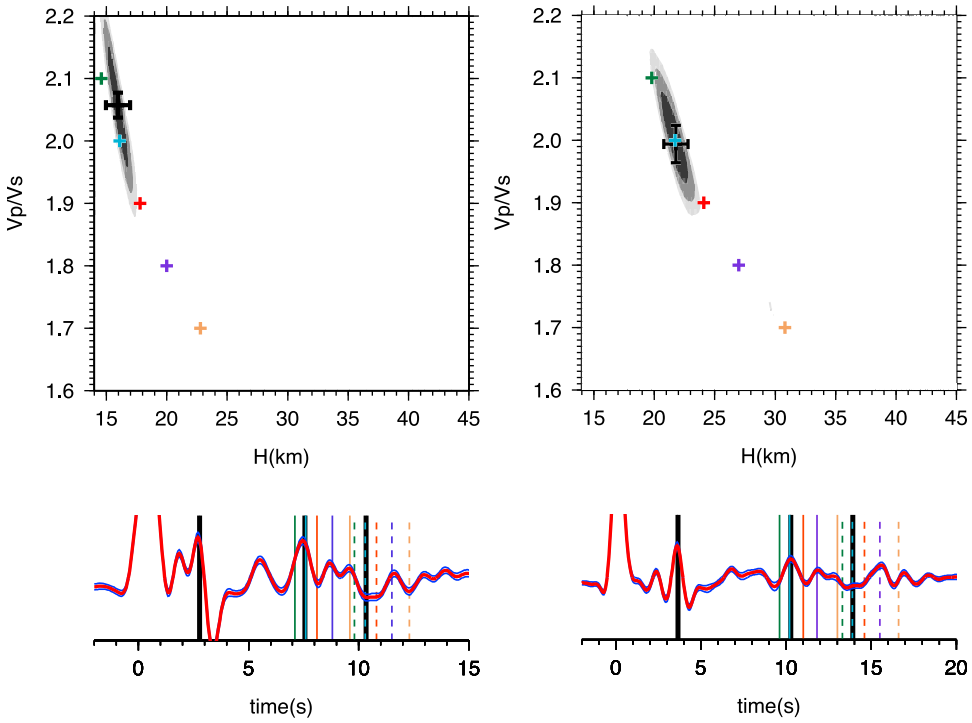

Figure 7. H-κ estimates of crustal thickness for (left) AFME and (right) FINE. Small colored crosses show predicted H-κ solutions for a range of V_P/V_S assuming a fixed *Ps* arrival time of 2.7 s (AFME) and 3.6 s (FINE) and an average crustal V_P of 6.15 km s^{-1}. Solid and dashed colored lines in the bottom panels show the predicted *PpPs* and *PpSs*/*PsPs* arrival times based on a range of V_P/V_S values (brown = 1.7, purple = 1.8, red = 1.9, blue = 2.0, green = 2.1). For other definitions see Figure 3 for definitions. It is evident that a high V_P/V_S is required to explain the H-κ results.

5.2. Southern and Central Afar

[22] Using refraction studies, *Makris and Ginzburg* [1987] show a flat horizontal Moho extending from the MER into Southern Afar, with a thickness of ~26 km. Our study supports this, but shows evidence of slightly thinner crust on the western side of the refraction profile (unfortunately we have no stations to the east) (Figure 5). This flat Moho extends until ~11.5° N, where the MER terminates against the Tendaho-Gob'a discontinuity (TGD) (Figure 5).

[23] North of latitude 12°N the Moho starts to shallow, thinning to ~17–23 km close to the DMH volcanic segments (Figure 5). However, regions of thicker crust are seen southwest of the TGD (MILE, 33 ± 5 km) and east of DMH (e.g., KOZE, 28 ± 2 km).

[24] Within the MER and Afar the estimated crustal V_P/V_S are predominantly above 1.9. Figure 7 shows that such high V_P/V_S is required to explain the data. Figure 4 (top) (after *Thompson et al.* [2010]) illustrates that any V_P/V_S above 1.9 cannot be achieved by a simple change in rock composition. To obtain such high V_P/V_S ratios, some fluid must be present (where fluid exists, *S*-wave velocity decreases more than *P*-wave, thus increasing V_P/V_S) [*Watanabe*, 1993]. It is hard to estimate the amount of melt needed as seismic velocity depends not just on melt fraction, but also on its geometry [*Kendall*, 2000] and attenuation mechanism (i.e. grain boundary relaxation [Faul et al., 2004] or melt squirt [*Hammond and Humphreys*, 2000]). However, such high V_P/V_S indicates that partial melt in the crust is ubiquitous throughout Afar. Volcanism has been active in the region for the past 30 Myrs, suggesting that magma intrusion has occurred across a ~300 km wide area over this time period.

[25] *Berckhemer et al.* [1975] estimated V_P/V_S for the upper crust (1.78 ± 0.004) based on local seismicity along Berckhemer profile 5 (Figure 1). Additionally, *Belachew et al.* [2011] estimated an average V_P/V_S for Afar and the adjacent margins of 1.8 again from local events that traverse the mid- to upper crust [*Belachew et al.*, 2011]. This is an average across all of Afar and the presence of magma injection into the upper crust beneath Afar

magmatic segments [*Ayele et al.*, 2007; *Ebinger et al.*, 2008; *Ayele et al.*, 2009; *Keir et al.*, 2009a; *Hamling et al.*, 2009; *Grandin et al.*, 2010, 2011; *Belachew et al.*, 2011] means a high upper crustal V_P/V_S would be expected in these regions (similar to that shown in the MER from crustal tomography [*Daly et al.*, 2008]). However we have no seismic stations directly above the magmatic segments, and thus cannot resolve this. Instead, our estimates are sensitive to the off-axis Afar structure where upper crustal V_P/V_S appears to be lower. In these regions the cause of high V_P/V_S, most likely partial melt, must predominantly be located in the lower crust. The area to the south of the TGD and east of DMH show a V_P/V_S below 1.9 and these regions coincide with thicker crust (Figure 5). This region has been imaged using seismic tomography [*Bastow et al.*, 2008], and even though it is on the edge of the array, it has fast velocities (relative to other parts of the rift) at upper mantle depths (75 km) [*Bastow et al.*, 2008]. Preliminary results for seismic tomography using the new Afar seismic array constrain this further and show this fast velocity region to be coincident with the region of thick crust and lower V_P/V_S [*Hammond et al.*, 2009], implying that lower degrees of melt are present in these regions.

5.3. Northern Afar

[26] North of latitude 13°N the crust thins sharply reaching 16 ± 1 km thick beneath AFME (Figure 5). Estimates of V_P/V_S are above or close to 2.0 at all stations.

[27] In Afar the regions with high V_P/V_S (>2.0) generally correlate with active volcanoes (Figure 4). This correlation between high V_P/V_S and volcanoes suggests that the lower crust close to the rift axis contains significant amounts of melt, likely feeding magmatic activity in the rift system.

[28] Two places show high V_P/V_S (>2.0) but little active volcanism. One is located close to ~40°E, 11°N (Figure 4). Interestingly, this anomalous signal lies directly below the Dahla Basalts, volcanics mapped as old magmatic segments associated with the early stages of Nubia-Arabia breakup in the late Miocene [*Wolfenden et al.*, 2005] (Figures 1 and 4). This suggests that partial melt is present in the lower crust beneath old rift structures. The other is located close to station ABAE (13.5°N, 40°E), and lies directly above a region of anomalously high, relatively deep off-axis seismicity [*Belachew et al.*, 2011; *Keir et al.*, 2011b]. Additionally, shear wave splitting from these events suggests the crust here is seismically anisotropic, possibly pointing to oriented melt in the crust beneath this region [*Keir et al.*, 2011b].

6. Receiver Function Migration

[29] To understand the lateral variation in crustal structure we produce common conversion point (CCP) images of crustal structure along 4 profiles through Afar (Figure 8). Following the methodology of *Angus et al.* [2006, 2009] we back-project the receiver function energy along the IASP91 raypath. The IASP91 velocity model is modified for the $H-\kappa$ results, creating an individual velocity model for each seismic station. The Moho depth is changed to fit H, and the shear wave velocity is calculated using κ. In all cases the mantle P-wave velocity is reduced to 7.6 km s^{-1} and the mantle V_P/V_S is set to 1.8. Thus the velocity model used in the migration varies across the array allowing for a more accurate treatment of lateral variations in crustal structure. The back projected RF amplitude is binned into lateral and depth bins. Lateral bins are calculated every 10 km and have a radius of 30 km (thus bins overlap). Profiles A (northern half) and B coincide with the refraction profiles of *Berckhemer et al.* [1975], while profile C and D show cross sections through parts of Afar not sampled previously (Figure 8).

6.1. Profile A

[30] This profile runs from south to north starting near station HYNE on the southeastern plateau and ending in northernmost Afar (Figure 8). Thick (>35 km) crust exists beneath the southeastern plateau. Coverage resumes in the region near the triple junction close to the Djibouti border where the crust is relatively thick (~30 km). The crust gradually thins northward reaching a thickness of 25 km at a latitude of 13°N, at which point the crust rapidly thins to ~16 km (a ~10 km decreases in depth over 20 km laterally). The V_P/V_S increases dramatically to over 2.0 at this latitude.

6.2. Profile B

[31] This profile runs from west to east starting on the western plateau, and running across Afar to the edge of the Danakil microplate (Figure 8). Crust is >35 km beneath the western plateau, but is marked by a high V_P/V_S. It gradually thins toward Afar reaching ~22 km close to 39.5°E, where the V_P/V_S remains above 2.0. This is close to the location of the Dahla basalts, eruptions thought to be due to late Miocene rifting [*Wolfenden et al.*, 2005].

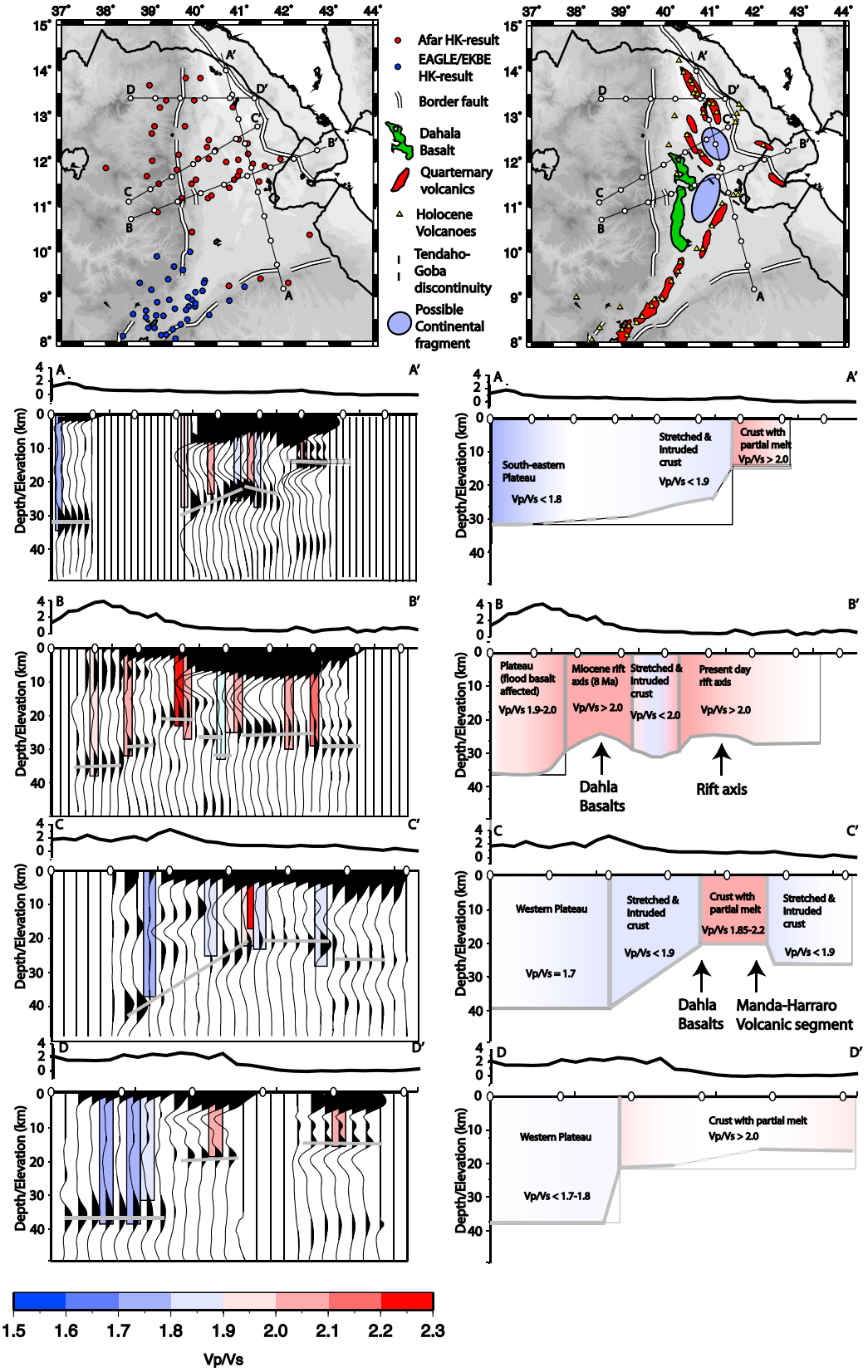

Figure 8. (first row, left) Map showing the location of the CCP profiles with station locations. (first row, right) Map showing the location of profiles with major geological features. See key for details. (bottom four rows) CCP migrated receiver functions along the four profiles shown above.

Further east along the profile (~40.5°E) the crust thickens to ~30 km, which is associated with a reduction of V_P/V_S (station MILE, V_P/V_S = 1.88 ± 0.11). This also coincides with faster velocities in the lithosphere seen in seismic tomography [*Hammond et al.*, 2009]. However, the thick crust is localized in lateral extent. Moving eastward (~41.0°E) the crust thins to ~23 km in the vicinity of the current rift axis and the V_P/V_S rises to ~2.0.

6.3. Profile C

[32] This profile runs from west to east starting near Wuchale on the western plateau and across the DMH volcanic segment, the location of recent magmatic activity [*Ayele et al.*, 2007; *Ebinger et al.*, 2008; *Ayele et al.*, 2009; *Keir et al.*, 2009a; *Hamling et al.*, 2009; *Grandin et al.*, 2010, 2011; *Belachew et al.*, 2011]. The profile terminates on the eastern side of the rift, close to the Danakil block margin (Figure 8). The western plateau is characterized by thick crust (~40 km), but in this case V_P/V_S is lower (<1.9) than that seen further south close to profile B. A coherent mid-crustal RF signal is present at ~20 km depth; similar to the depth of a mid-crustal discontinuity delineating upper and lower crust, imaged in refraction studies further south on the plateau [*Makris and Ginzburg*, 1987]. The crust gradually thins into Afar, reaching ~20 km at ~40°E. The mid-crustal discontinuity also shallows, but does not seem to be present east of 40°, the edge of the western plateau. This could be due to sediment reverberations masking the signal, or could be due to the velocity structure in the crust. This is further explored later in the paper. The crust remains at this thickness for ~100 km until it thickens to ~26 km just east of DMH. The western edge of this thin crust is again the location of Dahla basalts, the late Miocene volcanism [*Wolfenden et al.*, 2005], and the eastern edge of the thin crust is the location of the current rift axis (DMH). Once again the highest values of V_P/V_S (>2.0) exist where the crust is thinnest.

6.4. Profile D

[33] This profile runs from west to east from the western plateau and across northern Afar (Figure 8). Thick (~38 km) crust exists beneath the plateau, which sharply thins to <20 km at ~39.5°E. This thinning occurs over ~30 km. Again, toward the east thin crust coincides with the highest V_P/V_S. The crust continues to thin, reaching a minimum of 16 ± 1 km close to the Afdera/Erte Ale volcanic segments.

7. Grid-Search Inversion

[34] The H-κ method gives us estimates of the crustal thickness (Figure 5) and bulk V_P/V_S (Figure 4), and CCP stacks highlight changes in lateral structure (Figure 8). However, if we want to identify mid-crustal discontinuities, in particular how the lower and upper crust change, we must model the RF waveforms. The arrival times of conversions depends mainly on the *S*-wave velocity structure, depth of the discontinuities and V_P/V_S. As a result RF modeling can provide non-unique solutions [*Ammon et al.*, 1990]. In this study we construct a simple grid search inversion [*Lodge and Helffrich*, 2009]. We test the ability of the simple crustal model of *Prodehl and Mechie* [1991] to explain the RFs (where the RFs have a maximum frequency of 1.0 Hz), and thus constrain how the internal crustal structure varies throughout Afar.

[35] Many stations lie above sediments, pyroclastics, and lava flows of thickness 2 km or more [*Berckhemer et al.*, 1975; *Behle et al.*, 1975; *Makris and Ginzburg*, 1987; *Lemma et al.*, 2010]. In these cases, even though the Moho conversion is clear, the mid-crustal structure is often masked by energy reverberating in these shallow layers. Three stations (AFME, SILE, FINE) were deployed in soil or cairns above rhyolites and basalts thus minimizing sediment effects. As a result, only three stations in Afar were unambiguously modeled, but their geographical spread means they give an indication of the evolution of crust throughout Afar (Figure 1). Station FINE is located west of the DMH in central Afar above 22 ± 1 km thick crust and V_P/V_S of 1.99 ± 0.03, typical of the region between the Miocene rift axis and the current rift axis (Figure 1). Station SILE is located west of DMH in central Afar above 24 ± 2 km thick crust and V_P/V_S of 2.00 ± 0.08, typical of the thicker crust present east of the current rift axis (Figure 1). Station AFME is located north of SILE, on the Afdera volcanic segment in northern Afar above 16 ± 1 km thick crust and V_P/V_S of 2.06 ± 0.01, close to the region of rapid crustal thinning and above some of the thinnest crust imaged in this study (Figure 1).

[36] We split the 1D model into 5 layers, layers 1 and 2 represent the sediment and lava cover rocks, layer 3 is the upper crust, layer 4 is the lower crust

Table 2. Model Parameters: All Model Parameters Searched in the Grid-Search Inversion[a]

Station	Layer 1			Layer 2			Layer 3			Layer 4			Layer 5	
	V_P	V_P/V_S	H (km)	V_P	V_P/V_S	H (km)	V_P	V_P/V_S	H (km)	V_P	V_P/V_S	H (km)	V_P	V_P/V_S
AFME	3.35	1.60–2.00	0.0–3.0	4.5	1.60–2.00	0.0–3.0	6.1	1.7–1.9	0.0–6.0	6.9	1.70–2.50	0.0–16.0	7.6	1.80–2.50
(4461315)	-	(0.05)	(0.5)	-	(0.05)	(0.5)	-	0.05	(1.0)	-	(0.05)	(1.0)	-	(0.05)
FINE	2.2–3.4	1.70–1.90	0.0–3.0	4.1–4.5	1.70–1.90	0.0–3.0	6.1–6.5	1.7–1.9	0.0–14.0	6.6–7.2	1.70–2.50	0.0–24.0	7.6	1.80–2.20
(27322500)	(0.4)	(0.05)	(1.0)	(0.4)	(0.05)	(1.0)	(0.2)	(0.05)	(2.0)	(0.3)	(0.05)	(2.0)	-	(0.05)
SILE	3.35	1.60–2.00	0.0–3.0	4.5	1.60–2.00	0.0–3.0	6.1	1.7–1.9	0.0–14.0	6.95	1.70–2.50	0.0–26.0	7.6	1.80–2.20
(17673330)	-	(0.05)	(0.5)	-	(0.05)	(0.5)	-	0.05	(1.0)	-	(0.05)	(1.0)	-	(0.05)

[a]Number in brackets after station names relates to the number of models searched which lie within H-κ constraints. Numbers in brackets beneath parameters represent the spacing used in the grid-search for each parameter. Note, station FINE often has larger spacing to reduce the number of models to a reasonable number.

and layer 5 is the mantle. For stations SILE and AFME we fix *P*-wave velocities based on the nearby refraction profiles of *Berckhemer et al.* [1975] and *Makris and Ginzburg* [1987]. For station FINE, no nearby refraction profiles exist, so *P*-wave velocity is allowed to vary in all layers (see Table 2 for details). We allow two additional parameters to vary within each crustal layer; V_P/V_S, and thickness. V_P/V_S for the cover rocks is allowed to vary between 1.6 and 2.0 and V_P/V_S in the upper crust can vary between 1.7 and 1.9. This is based on the observation that the upper crust has a V_P/V_S of ~1.8 [*Berckhemer et al.*, 1975; *Belachew et al.*, 2011]. The V_P/V_S is allowed to vary between 1.8 and 2.5 in the lower crust and mantle. Thickness of the cover rocks (layers 1 and 2) was varied between 0 and 3 km. The upper crust and lower crust layers were varied on a station by station basis. Table 2 shows the range of parameters searched for selected stations. Density is calculated using $\rho = 1.72 + 0.337V_S$ [*Christensen and Salisbury*, 1975] for crustal rocks and $\rho = (V_P + 1.87)/3.05$ [*Birch*, 1961] for mantle rocks. We model the first 15 s at AFME, 18 s at FINE and SILE. As the modeling is non-unique some constraints are applied to the model space. The average crustal depth and V_P/V_S must lie within the error bounds of the H-κ study.

[37] We calculate a chi-squared (χ^2) misfit for each data-synthetic RF fit (see *Lodge and Helffrich* [2009] for details). *Lodge and Helffrich* [2009] then calculate a $\Delta\chi^2$ value based on the number of degrees of freedom of the model. We have 9 degrees of freedom for SILE and AFME and 13 degrees of freedom for FINE, which equates to $\Delta\chi^2$ of 16.92 (SILE, AFME) and 22.36 (FINE) [*Press et al.*, 1992] for 95% confidence intervals. However, due to the simple modeling we often do not achieve misfit values below the $\Delta\chi^2$. The best fitting models have a χ^2 value of 30.53 (SILE), 24.91 (FINE) and 35.59 (AFME), which means they satisfy the $\Delta\chi^2$ for 99.99%, 99% and 99.999% confidence intervals respectively (Figure 9). It is evident that we have little constraint on the V_P/V_S in the cover rocks. Also, we do not constrain the upper crust V_P/V_S ratio well. However, it is evident that the data are particularly sensitive to the thickness in all layers, the V_P/V_S in the lower crust and mantle and the velocity contrast across all layers (Figure 9).

[38] Figure 10 and Table 3 show results from the 3 stations modeled. While the model fits are adequate (for example, the time 6–10 s at station AFME is poorly fit), the simple models based on previous controlled source interpretations have reasonable fits. These models show cover rock thickness of

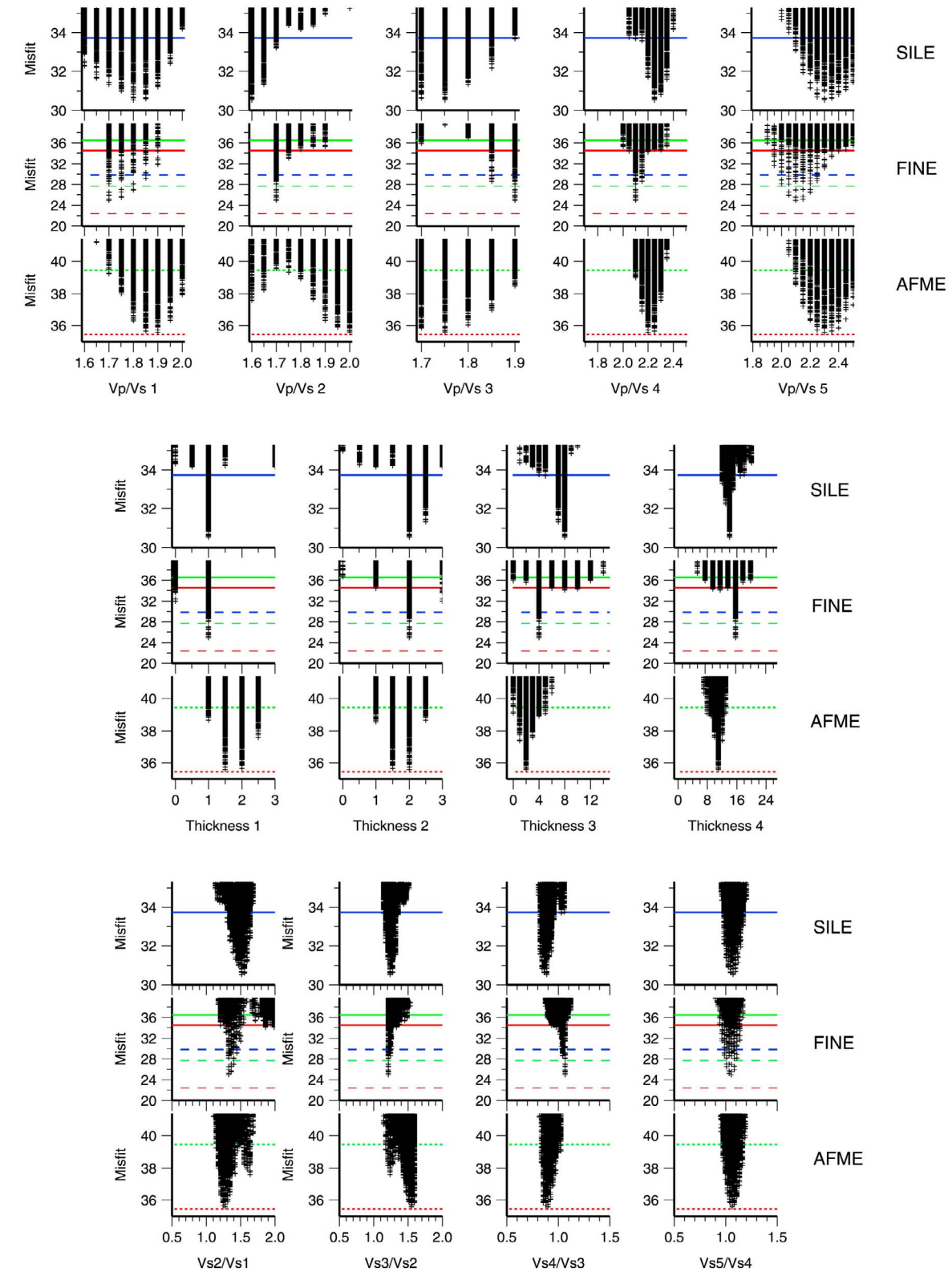
Misfit
SILE
FINE
AFME
Vp/Vs 1
Vp/Vs 2
Vp/Vs 3
Vp/Vs 4
Vp/Vs 5
Thickness 1
Thickness 2
Thickness 3
Thickness 4
Vs2/Vs1
Vs3/Vs2
Vs4/Vs3
Vs5/Vs4
95%
99%
99.5%
99.9%
99.95%
99.99%
99.995%
99.999%

Figure 9

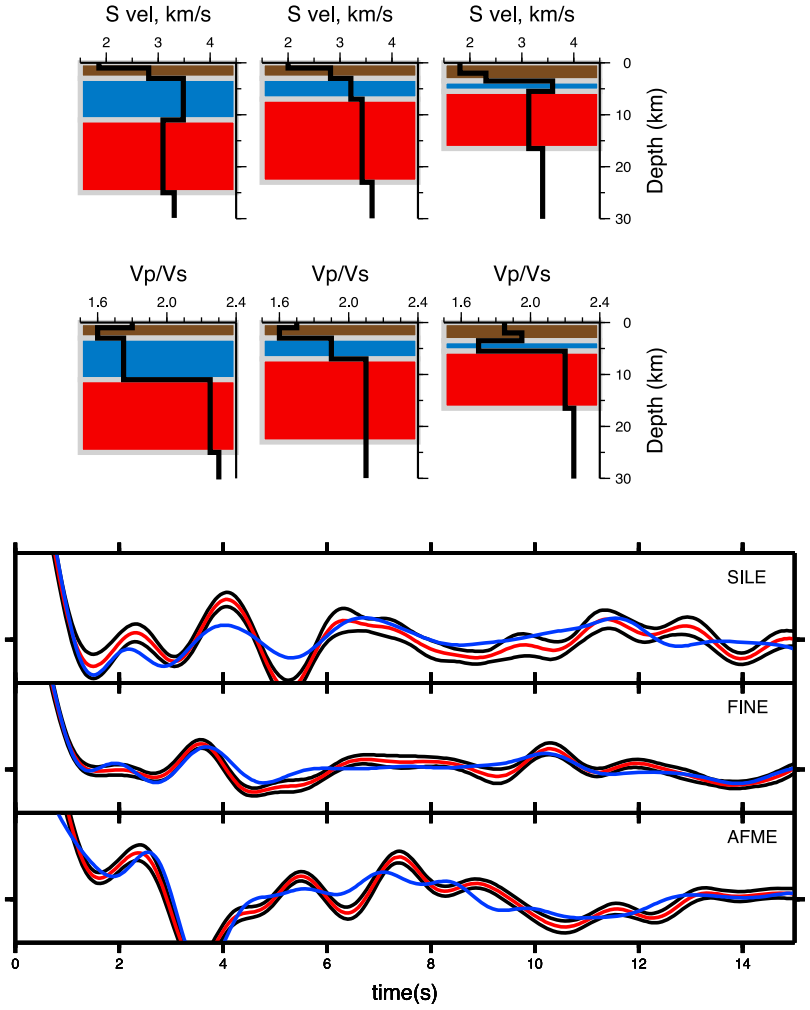

Figure 10. Final grid-search models for SILE, FINE and AFME. The *S*-wave velocity model is shown by the black solid line in the top plot (left SILE, middle FINE, right AFME) and the V_P/V_S model is shown by the black line in the middle plots. In these plots brown shading shows the cover rocks (CR), blue shading shows the upper crust (UC) and red shading shows the lower crust (LC). The three RF plots at the bottom show the data derived receiver function (red line) along with the jackknife derived 95% confidence interval (thin black lines), and the modeled RF (blue line).

4 km overlying an upper crust of 8 km and a 12 km lower crust beneath station SILE. FINE shows 3 km of cover rocks overlying a 4 km thick upper crust and 16 km thick lower crust. AFME shows 3.5 km of cover rocks overlying a 2 km thick upper crust and 11 km thick lower crust (Table 3). In all three cases, the lower crust has a V_P/V_S above 2.0. In the case of AFME and SILE, V_P/V_S is so high that the lower crust has a lower shear wave velocity than the overlying upper crust (Figure 9). This explains why, even though a discrete *P*-wave velocity jump is observed in the refraction studies in Afar between upper and lower crust, little to no energy is present in the RFs at times associated with this velocity jump. Even though the *P*-wave velocity increases, the *S*-wave velocity remains relatively unchanged resulting in little converted energy (FINE), or the *S*-wave velocity decreases resulting in negative peaks (AFME, SILE) (Figure 9). This suggests that the lower crust contains appreciable

Figure 9. Sensitivity analysis of 9 parameters searched in the grid-search inversion. (top three rows) The V_P/V_S ratios for all layers in the model for the three seismic stations. (middle three rows) The thickness of the top four layers for all stations (the fifth layer is a half-space). (bottom three rows) The velocity contrast across all layers. Crosses show the top 5000 models. Colored lines show the $\Delta\chi^2$ misfit value for confidence intervals ranging from 95% to 99.999%. It is evident that this inversion is particularly sensitive to thickness of all layers, V_P/V_S in layers 4 and 5 (lower crust and mantle) and the velocity contrast across all layers.

Table 3. Best Fitting Velocity Models for AFME, FINE and SILE From the Grid-Search Inversion

Layer Number	Layer Description	V_P (km s^{-1})	V_S (km s^{-1})	ρ (kg m^{-3})	Depth (km)
		AFME			
1	Cover Rocks	3.4	1.8	2.33	2.0
2	Cover Rocks	4.5	2.3	2.50	3.5
3	Upper Crust	6.1	3.6	2.92	5.5
4	Lower Crust	6.9	3.1	2.78	16.5
5	Mantle	7.7	3.4	3.12	∞
		FINE			
1	Cover Rocks	3.4	2.0	2.39	1.0
2	Cover Rocks	4.5	2.8	2.67	3.0
3	Upper Crust	6.1	3.2	2.80	7.0
4	Lower Crust	7.2	3.4	2.88	23.0
5	Mantle	7.6	3.6	3.10	∞
		SILE			
1	Cover Rocks	3.4	1.9	2.35	1.0
2	Cover Rocks	4.5	2.8	2.67	3.0
3	Upper Crust	6.1	3.5	2.89	11.0
4	Lower Crust	7.0	3.1	2.76	25.0
5	Mantle	7.6	3.3	3.10	∞

amounts of partial melt, possibly highlighting a lower crustal 'hot zone', a result of multiple injection of sills into the lower crust [*Annen et al.*, 2006]. It is unclear as to whether this melt filled lower crust is new mafic crustal material, or is due to magmatic intrusions into older continental crust. The mantle also shows high V_P/V_S suggesting that partial melt is present in the uppermost mantle.

[39] The upper crustal variations give a second insight into the evolution of crust in Afar. Stations FINE and AFME show thin upper crustal layers (4 and 2 km respectively). Indeed, AFME shows only 2 km thick upper crust which is arguably on the limit of resolution for the RF technique. Conversely, station SILE shows a relatively thick upper crust of 8 km. This station lies to the east of the current rift axis, above thicker crust seen in the H-κ stacking and CCP migrations (Figures 5 and 8). This suggests, along with the faster seismic velocities seen at upper-mantle depths (~75 km) [*Hammond et al.*, 2009], that this region has undergone less stretching than the region west of it. This station does have a high V_P/V_S of 2.00 ± 0.08, implying partial melt in the lower crust caused by mafic intrusions. However, other stations close to this show lower V_P/V_S (KOZE (~25 km from SILE), H = 28 ± 2, V_P/V_S = 1.84 ± 0.07, BREE (~27 km from SILE), H = 26 ± 1, V_P/V_S = 1.84 ± 0.02) suggesting that not all the lower crust in this region has undergone the same alteration. Additionally, estimates of crustal structure from controlled source studies show evidence of 8 km thick upper crust near the Danakil plate [*Makris and Ginzburg*, 1987] and in the Southern Red Sea [*Mechie et al.*, 1986] (Figure 2). This evidence supports the idea that a significant continental component of crust exists to the east of the current rift axis, the presence of mafic material in the lower crust means that some focus of magmatic activity may be present between here and the Danakil, but a lack of data toward Eritrea means this can not be tested.

8. Implications of Crustal Structure to the Evolution of Afar

[40] *Tesfaye et al.* [2003] suggest that no triple junction existed in Afar until 10 Ma. At that time it was located close to the southernmost tip of the Afar depression (~10°N, 40–41°E) along a zone of deformation labeled the arcuate accommodation zone (Figure 11). Due to the difference in spreading rates between Nubia-Arabia (~16 mm yr^{-1}), Arabia-Somali (~18 mm yr^{-1}) [*Vigny et al.*, 2006] and Nubia-Somalia (3–6 mm yr^{-1}) [*Bilham et al.*, 1999; *Bendick et al.*, 2006], the triple junction in Afar has migrated northeast ~160 km in 10 Myr [*McKenzie and Morgan*, 1969; *Tesfaye et al.*, 2003; *Kalb*, 1995]. The migration of the triple junction suggests that the plate boundaries must also move over time. This is evident in the geological record, where the MER has propagated north-eastward, cutting through old structures [*Tesfaye et al.*, 2003; *Wolfenden et al.*, 2004, 2005; *Keir et al.*, 2011a], and it has also been suggested that the GOA rift axis has migrated northward [*Manighetti et al.*, 1998; *Audin et al.*, 2004] as it has evolved through time. We have little data coverage on the MER or GOA rifts in Afar, but the asymmetrical nature of crustal thickness around the southern RSR suggest that this arm of the triple junction has moved eastward to accommodate the migrating triple junction.

[41] As the triple junction migrated north-eastward, the Red Sea rift, which originated in a north-south orientation [*Wolfenden et al.*, 2005], has had to rotate into the present north-west/south-east orientation (Figure 11). RF profiles show structure which supports this hypothesis, with thin crust underlying the Miocene rift axis and the current rift axis (Figure 8). Profile C shows thicker crust west of the Miocene rift axis and east of the current rift axis (Figure 8). If the rift axis had not migrated, then crustal structure would be expected to be symmetric around the current rift axis. It seems

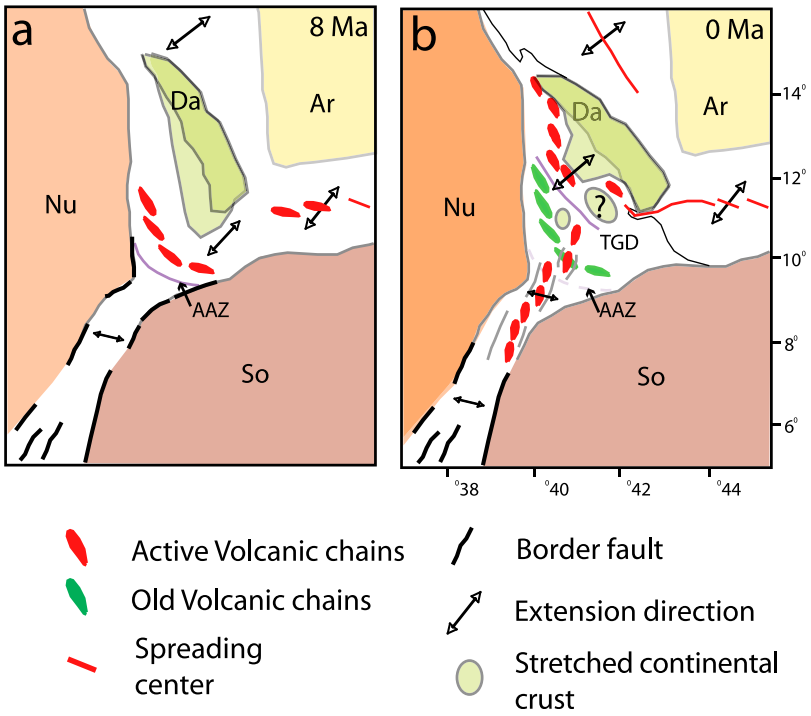

Figure 11. Cartoons showing the proposed models of the Afar depression at (a) 8 Ma and (b) present-day (adapted from *Audin et al.* [2004] and *Wolfenden et al.* [2004]). Light green shading indicates the Danakil block margins of *Eagles et al.* [2002] (labeled Da), and the proposed larger margins and continental fragments proposed in this study. Note the margins proposed here are not well constrained, and is included to illustrate that other fragments of continental material possibly exist within the Afar depression. AAZ, Arcuate Accommodation Zone; TGD, Tendaho-Gob'a Discontinuity.

likely that the rift axis has migrated eastward from the Miocene rift axis to the present-day rift axis.

[42] Thin crust (<26 km) is present north and west of ~41°E, ~12°N (Figures 5 and 8). A region of thin crust (<26 km) exists beneath the Dahla basalts at ~40°E, ~11.5°N, highlighting the Miocene rift axis [*Wolfenden et al.*, 2005]. If the rift axis had migrated uniformly through time, the region between the Miocene rift and the current rift axis should contain evidence for a significant amounts of partial melt, as is the case in the rest of Afar. A region of thicker crust and lower V_P/V_S (station MILE, $H = 33 \pm 5$, $V_P/V_S = 1.88 \pm 0.11$) and faster upper mantle velocity [*Bastow et al.*, 2008; *Hammond et al.*, 2009] exists between the Miocene and current rift axes (Figures 4, 5, and 8). The extent of the thicker crust is hard to determine from the distribution of sensors presented here, but its presence suggests that the rift may have jumped as the triple junction migrated north-eastward. The timing of this jump is hard to determine, however paleolake chronology in Afar shows a south to north migration of paleolakes [*Kalb*, 1995] coincident in location with the basins and volcanics associated with upper Miocene rifting [*Wolfenden et al.*, 2005] until ~3 Ma. The more recent lakes, less than ~3 Ma are oriented on the current NW-SE Red Sea rift axis [*Kalb*, 1995].

[43] Ridges have often been observed to migrate as a series of rift jumps, which are commonly associated with microcontinent formation [*Müller et al.*, 2001]. The region of thicker crust, fast velocities and lower Vp/Vs (located close to the town of Mile), may be a small region of continental lithosphere, that has been left isolated in the largely oceanic Afar crust.

[44] On the eastern side of the current rift axis there is another region of thicker crust (24–28 km), and lower Vp/Vs (1.84–2.00), suggesting that this region has undergone a smaller degree of deformation, and retains a more continental signature. This may explain why *Berckhemer et al.* [1975] and *Makris and Ginzburg* [1987] suggest the whole of Afar is made-up of stretched continental material, as their profile samples the region east of the rift axis (Figure 1). We propose that west of the current rift axis is predominantly mafic material, with oceanic affinities, whereas east of the DMH

rift zone lies continental material (Figure 8). *Eagles et al.* [2002] acknowledge that south of the Alayta volcanic chain (~41°E, 13°N) it is hard to determine the Danakil plate boundary due to more recent rift structures. We propose that much of the region between the currently assumed Danakil margin, and the DMH rift axis is in fact continental material. Unfortunately a lack of data close to the Ethiopia/Eritrea border means it is not clear if this material is connected to the Danakil block, or isolated. Future deployments in Eritrea will hopefully shed more light on this.

9. Conclusions

[45] This RF study provides new estimates of crustal structure in the Afar depression, Ethiopia. We have shown that crust beneath this rift-rift-rift triple junction thins from ~26 km in the south to ~16 km in the north. It is bounded by thick crust, ~40–45 km beneath the western plateau and ~35 km beneath the southeastern plateau (Figure 5). We have shown that almost all Afar crust must contain significant amounts of melt, located in the lower crust, and particularly beneath regions of thinner crust (Figures 5–8). The regions of melt are focused along current (based on seismicity [*Keir et al.*, 2006; *Ebinger et al.*, 2008; *Keir et al.*, 2009a; *Belachew et al.*, 2011]) and past plate boundaries [*Wolfenden et al.*, 2005]. The large degrees of partial melt present in these locations supports the idea that magma injection into the upper crust from lower crustal reservoirs plays an important role in late stage rifting, accommodating a large part of the strain associated with the breakup [*Ebinger and Casey*, 2001]. The presence of partial melt beneath most of Afar implies that magma intrusion has been active across most of the region over the last 30 Myrs. These persistent magma intrusions, combined with dynamic support of mantle upwelling, may explain why the incipient break-up zones in Afar remain above sea level [e.g., *Ebinger and Hayward*, 1996; *Lithgow-Bertelloni and Silver*, 1998].

[46] By mapping out the crustal structure characteristics of past and present plate boundaries, we show evidence for rift migration of the RSR arm of the triple junction. The rift had a N-S orientation ~8 Ma [*Wolfenden et al.*, 2005], but as the triple junction has migrated north-eastward [*Wolfenden et al.*, 2004; *Tesfaye et al.*, 2003], the RSR has migrated to a more NW-SE orientation (Figure 11). This has resulted in small blocks of material to be isolated in the largely mafic Afar crust (Figure 8). Eastward of the DMH rift segment lies continental material which may be connected to the Danakil block, or may be isolated due to GOA rift activity [*Manighetti et al.*, 1998].

Acknowledgments

[47] We would like to thank Addis Ababa University, the Ethiopian Federal Government and Afar National Regional State Government and Ethioder tour and travel for support throughout the experiment. Seismic equipment was loaned from SEIS-UK and IRIS-Pascal. Two anonymous reviewers are thanked for their insightful comments which improved the paper. Fieldwork and J.O.S.H. was funded by NERC grants NE/E007414/1 and NE/D008611/1 and NSF grant EAR-0635789. All those involved in fieldwork are thanked for their efforts.

References

Ammon, C. J., G. E. Randall, and G. Zandt (1990), On the nonuniqueness of receiver function inversions, *J. Geophys. Res.*, *95*(B10), 15,303–15,318.

Angus, D. A., D. C. Wilson, E. Sandvol, and J. F. Ni (2006), Lithospheric structure of the Arabian and Eurasian colliern Turkey from *S*-wave receiver functions, *Geophys. J. Int.*, *166*, 1335–1346.

Angus, D. A., J. Kendall, D. C. Wilson, D. J. White, S. Sol, and C. J. Thomson (2009), Stratigraphy of the Archean western Superior Province from P- and S-wave receiver functions: Further evidence for tectonic accretion?, *Phys. Earth Planet. Inter.*, *177*, 206–216.

Annen, C., J. Blundy, and R. Sparks (2006), The genesis of intermediate and silicic magmas in deep crustal hot zones, *J. Petrol.*, *47*(3), 505.

Audin, L., X. Quidelleur, E. Coulié, V. Courtillot, S. Gilder, I. Manighetti, P. Gillot, P. Tapponnier, and T. Kidane (2004), Palaeomagnetism and K-Ar and 40Ar/39Ar ages in the Ali Sabieh area (Republic of Djibouti and Ethiopia): constraints on the mechanism of Aden ridge propagation into southeastern Afar during the last 10 Myr, *Geophys. J. Int.*, *158*(1), 327–345.

Ayele, A., G. Stuart, and J. Kendall (2004), Insights into rifting from shear wave splitting and receiver functions: an example from Ethiopia, *Geophys. J. Int.*, *157*(1), 354–362.

Ayele, A., E. Jacques, M. Kassim, T. Kidane, A. Omar, S. Tait, A. Nercessian, J. de Chabalier, and G. King (2007), The volcano-seismic crisis in Afar, Ethiopia, starting September 2005, *Earth Planet. Sci. Lett.*, *255*(1–2), 177–187.

Ayele, A., D. Keir, C. Ebinger, T. J. Wright, G. W. Stuart, W. R. Buck, E. Jacques, G. Ogubazghi, and J. Sholan (2009), September 2005 mega-dike emplacement in the Manda-Harraro nascent oceanic rift (Afar depression), *Geophys. Res. Lett.*, *36*, L20306, doi:10.1029/2009GL039605.

Barberi, F., R. Santacroce, and R. Varet (1975), Structural evolution of the Afar Triple Junction, in *Afar Depression of Ethiopia: Proceedings of an International Symposium on the Afar Region and Related Rift Problems, Held in Bad Bergzabern, FR Germany, April 1–6, 1974*, pp. 89–107, Schweizerbart, Stuttgart, Germany.

Barrat, J. A., J. L. Joron, R. N. Taylor, S. Fourcade, R. W. Nesbitt, and B. M. Jahn (2003), Geochemistry of basalts from manda hararo, ethiopia: Lree-depleted basalts in central afar, *Lithos*, *69*(1–2), 1–13.

Bastow, I. D., and D. Keir (2011), The protracted development of the continent-ocean transition in Afar, *Nat. Geosci.*, *4*, 248–250.

Bastow, I. D., A. A. Nyblade, G. W. Stuart, T. O. Rooney, and M. H. Benoit (2008), Upper mantle seismic structure beneath the Ethiopian hot spot: Rifting at the edge of the African low-velocity anomaly, *Geochem. Geophys. Geosyst.*, *9*, Q12022, doi:10.1029/2008GC002107.

Bastow, I., S. Pilidou, J.-M. Kendall, and G. Stuart (2010), Melt-induced seismic anisotropy and magma assisted rifting in Ethiopia: Evidence from surface waves, *Geochem. Geophys. Geosyst.*, *11*, Q0AB05, doi:10.1029/2010GC003036.

Bastow, I. D., D. Keir, and E. Daly (2011), The Ethiopia Afar Geoscientific Lithospheric Experiment (EAGLE): Probing the transition from continental rifting to incipient sea-floor spreading, in *Volcanism and Devolution of the African Lithosphere*, edited by L. Beccaluva, G. Bianchini, and M. Wilson, *Spec. Pap. Geol. Soc. Am.*, *478*, 1–26.

Behle, A., J. Makris, J. Baier, and N. Delibasis (1975), Salt thickness near Dallol (Ethiopia) from seismic reflection measurements and gravity data, in *Afar Depression of Ethiopia: Proceedings of an International Symposium on the Afar Region and Related Rift Problems, Held in Bad Bergzabern, FR Germany, April 1–6, 1974*, pp. 156–167, Schweizerbart, Stuttgart, Germany.

Belachew, M., C. J. Ebinger, D. Cote, D. Keir, J. Rowland, J. O. S. Hammond, and A. Ayele (2011), Comparison of dike intrusions in an incipient seafloor spreading segment in Afar, Ethiopia: Seismicity perspectives, *J. Geophys. Res.*, *116*, B06405, doi:10.1029/2010JB007908.

Bendick, R., S. McClusky, R. Bilham, L. Asfaw, and S. Klemperer (2006), Distributed Nubia–Somalia relative motion and dike intrusion in the Main Ethiopian Rift, *Geophys. J. Int.*, *165*(1), 303–310.

Berckhemer, H., et al. (1975), Deep seismic soundings of the Afar region and on the highland of Ethiopia, in *Afar Depression of Ethiopia: Proceedings of an International Symposium on the Afar Region and Related Rift Problems, Held in Bad Bergzabern, FR Germany, April 1–6, 1974*, pp. 89–107, Schweizerbart, Stuttgart, Germany.

Beyene, A., and M. G. Abdelsalam (2005), Tectonics of the Afar Depression: A review and synthesis, *J. Afr. Earth Sci.*, *41*, 41–59.

Bilham, R., R. Bendick, K. Larson, P. Mohr, J. Braun, S. Tesfaye, and L. Asfaw (1999), Secular and tidal strain across the Main Ethiopian Rift, *Geophys. Res. Lett.*, *26*(18), 2789–2792.

Birch, F. (1961), Velocity of compressional waves in rocks to 10 kilobars, Part 2, *J. Geophys. Res.*, *66*, 2199–2224.

Buck, W. R. (2004), Consequences of asthenospheric variability on continental rifting, in *Rheology and Deformation of the Lithhosphere at Continental Margins*, edited by G. D. Karne et al., pp. 1–30, Columbia Univ. Press, New York.

Christensen, N. I. (1996), Poisson's ratio and crustal seismology, *J. Geophys. Res.*, *101*(B2), 3139–3156.

Christensen, N. I., and M. Salisbury (1975), Structure and constitution of the lower oceanic crust, *Rev. Geophys.*, *13*(1), 57–86.

Cornwell, D. G., G. D. Mackenzie, R. W. England, P. K. H. Maguire, L. M. Asfaw, and B. Oluma (2006), Northern Main Ethiopian Rift crustal structure from new high-precision gravity data, in *The Afar Volcanic Province Within the East African Rift System*, edited by G. Yirgu, C. J. Ebinger, and P. K. H. Maguire, *Geol. Soc. Spec. Publ.*, *259*, 307–321.

Cornwell, D. G., P. K. H. Magurie, R. W. England, and G. W. Stuart (2010), Imaging detailed crustal structure and magmatic intrusion across the Ethiopian rift using a dense linear broadband array, *Geochem. Geophys. Geosyst.*, *11*, Q0AB03, doi:10.1029/2009GC002637.

d'Acremont, E., S. Leroy, M.-O. Beslier, N. Bellahsen, M. Fournier, C. Robin, M. Maia, and P. Gente (2005), Structure and evolution of the eastern Gulf of Aden conjugate margins from seismic reflection data, *Geophys. J. Int.*, *160*, 869–890.

Daly, E., D. Keir, C. J. Ebinger, G. W. Stuart, I. D. Bastow, and A. Ayele (2008), Crustal tomographic imaging of a transitional continental rift: the Ethiopian rift, *Geophys. J. Int.*, *172*, 1033–1048.

Davidson, A., and D. C. Rex (1980), Age of volcanism and rifting in souhern Ethiopia, *Nature*, *283*, 657–658.

Dugda, M. T., and A. A. Nyblade (2006), New constraints on crustal structure in eastern Afar from the analysis of receiver functions and surface wave dispersion in Djibouti, in *The Afar Volcanic Province Within the East African Rift System*, edited by G. Yirgu et al., *Geol. Soc. Spec. Publ.*, *259*, 55–72.

Dugda, M. T., A. A. Nyblade, J. Julia, C. A. Langston, C. J. Ammon, and S. Simiyu (2005), Crustal structure in Ethiopia and Kenya from receiver function analysis: Implications for rift development in eastern Africa, *J. Geophys. Res.*, *110*, B01303, doi:10.1029/2004JB003065.

Dugda, M. T., A. A. Nyblade, J. Julia, C. A. Langston, C. J. Ammon, and S. Simiyu (2007), Thin lithosphere beneath the Ethiopian Plateau revealed by a joint onversion of Rayleigh wave group velocities and reciever functions, *J. Geophys. Res.*, *112*, B08305, doi:10.1029/2006JB004918.

Eagles, G., R. Gloaguen, and C. Ebinger (2002), Kinematics of the Danakil microplate, *Earth Planet. Sci. Lett.*, *203*, 607–620.

Ebinger, C. J., and M. Casey (2001), Continental breakup in magmatic provinces: an Ethiopian example, *Geology*, *29*, 527–530.

Ebinger, C. J., and N. J. Hayward (1996), Soft plates and hot spots: Views from Afar, *J. Geophys. Res.*, *101*, 21,859–21,876.

Ebinger, C. J., T. Yemane, G. WoldeGabriel, J. L. Aronson, and R. C. Walter (1993), Late Eocene–Recent volcanism and faulting in the southern main ethiopian rift, *J. Geol. Soc.*, *150*(1), 99–108.

Ebinger, C. J., D. Keir, A. Ayele, E. Calais, T. J. Wright, M. Belachew, J. O. S. Hammond, E. Campbell, and W. R. Buck (2008), Capturing magma intrusion and faulting processes during continental rupture: Seismicity of the Dabbahu (Afar) rift, *Geophys. J. Int.*, *174*, 1138–1152.

Ebinger, C., A. Ayele, D. Keir, J. Rwland, G. Yirgu, T. Wright, M. Belachew, and I. Hamling (2010), Length and timescales of rift faulting and magma intrusion: The Afar rifting cycle from 2005 to present, *Ann. Rev. Earth Planet. Sci.*, *38*, 437–464.

Efron, B. (1982), *The Jackknife, the Bootstrap and Other Resampling Plans*, Soc. for Ind. and Appl. Math., Philidelphia, Pa.

Efron, B., and R. Tibshirani (1991), Statistical data analysis in the computer age, *Science*, *253*(5018), 390.

Egloff, F., R. Rihm, J. Makris, Y. Izzeldin, M. Bobsien, K. Meier, P. Junge, T. Noman, and W. Warsi (1991), Contrasting structural styles of the eastern and western margins

of the southern Red Sea: The 1988 SONNE experiment, *Tectonophysics*, *198*(2–4), 329–353.

Faul, U., J. Gerald, and I. Jackson (2004), Shear wave attenuation and dispersion in melt-bearing olivine polycrystals: 2. Microstructural interpretation and seismological implications, *J. Geophys. Res.*, *109*, B06202, doi:10.1029/2003JB002407.

Garfunkel, Z., and M. Beyth (2006), Constraints on the structural development of Afar imposed by the kinematics of the major surrounding plates, in *The Afar Volcanic Province Within the East African Rift System*, edited by G. Yirgu, C. J. Ebinger, and P. K. H. Maguire, *Geol. Soc. Spec. Publ.*, *259*, 23–42.

Gaulier, J. M., X. LePichon, N. Lyberis, F. Avedik, L. Geli, I. Moretti, A. Deschamps, and H. Salah (1988), Seismic study of the crust of the northern Red Sea and Gulf of Suez, *Tectonophysics*, *153*, 55–88.

Grandin, R., A. Socquet, M. P. Doin, E. Jacques, J. B. de Chabalier, and G. C. P. King (2010), Transient rift opening in response to multiple dike injections in the manda hararo rift (Afar, Ethiopia) imaged by time-dependent elastic inversion of interferometric synthetic aperture radar data, *J. Geophys. Res.*, *115*, B09403, doi:10.1029/2009JB006883.

Grandin, R., et al. (2011), Seismicity during lateral dike propagation: Insights from new data in the recent manda hararo–Dabbahu rifting episode (Afar, Ethiopia), *Geochem. Geophys. Geosyst.*, *12*, Q0AB08, doi:10.1029/2010GC003434.

Hamling, I., A. Ayele, L. Bennati, E. Calais, C. Ebinger, D. Keir, E. Lewi, T. Wright, and G. Yirgu (2009), Geodetic observations of the ongoing Dabbahu rifting episode: New dyke intrusions in 2006 and 2007, *Geophys. J. Int.*, *178*(2), 989–1003.

Hammond, J. O. S., J. Kendall, G. W. Stuart, and C. J. Ebinger (2009), Seismic imaging of the crust and upper mantle beneath Afar, Ethiopia, *Eos Trans. AGU*, *90*(52), Fall Meet. Suppl., Abstract T31B-1808.

Hammond, J. O. S., J.-M. Kendall, D. Angus, and J. Wookey (2010), Interpreting spatial variations in anisotropy: Insights into the Main Ethiopian Rift from SKS waveform modelling, *Geophys. J. Int.*, *181*, 1701–1712.

Hammond, W., and E. Humphreys (2000), Upper mantle seismic wave velocity: Effects of realistic partial melt geometries, *J. Geophys. Res.*, *105*(B5), 10,975–10,986.

Harmon, N., D. W. Forsyth, R. Lamm, and S. C. Webb (2007), *P* and *S* wave delays beneath intraplate volcanic ridges and gravity lineations near the east pacific rise, *J. Geophys. Res.*, *112*, B03309, doi:10.1029/2006JB004392.

Hayward, N. J., and C. J. Ebinger (1996), Variations in along-axis segmentation of the Afar rift system, *Tectonics*, *15*(2), 244–257, doi:10.1029/95TC02292.

Hebert, L., and C. A. Langston (1985), Crustal thickness estimate at AAE (Addis-Ababa, Ethiopia) and NAI (Nairobi, Kenya) using teleseismic P-wave conversions, *Tectonophysics*, *111*(3–4), 299–327.

Helffrich, G. (2006), Extended-time multi-taper frequency domain cross-correlation receiver function estimation, *Bull. Seismol. Soc. Am.*, *96*, 344–347.

Kalb, J. E. (1995), Fossil Elephantoids, Awash paleolake basins, and the Afar triple junction, Ethiopia, *Palaeogeogr. Palaeoclimatol. Palaeoecol.*, *114*, 357–368.

Keir, D., G. W. Stuart, A. Jackson, and A. Ayele (2006), Local earthquake magnitude scale and seismicity rate for the Ethiopian rift, *Bull. Seismol. Soc. Am.*, *96*, 2221–2230, doi:10.1785/0120060051.

Keir, D., et al. (2009a), Evidence for focused magmatic accretion at segment centers from lateral dike injections captured beneath the Red Sea rift in Afar, *Geology*, *37*, 59–62, doi:10.1130/G25147A.1.

Keir, D., I. D. Bastow, K. A. Whaler, E. Daly, D. G. Cornwell, and S. Hautot (2009b), Lower crustal earthquakes near the Ethiopian rift induced by magmatic processes, *Geochem. Geophys. Geosyst.*, *10*, Q0AB02, doi:10.1029/2009GC002382.

Keir, D., C. Pagli, I. D. Bastow, and A. Ayele (2011a), The origins of Arabia: evidence from dike injection in the Ethiopian rift captured using InSAR and seismicity, *Tectonics*, *30*, TC2008, doi:10.1029/2010TC002785.

Keir, D., M. Belachew, C. J. Ebinger, J. Kendall, J. O. S. Hammond, G. W. Stuart, and A. Ayele (2011b), Mapping the evolving strain field in the Afar Triple Junction using crustal anisotropy, *Nat. Commun.*, *2*, Article 285, doi:10.1038/ncomms1287.

Kendall, J.-M. (2000), Seismic anisotropy in the boundary layers of the mantle, in *Earth's Deep Interior: Mineral Physics and Tomography From the Atomic to the Global Scale*, *Geophys. Monogr. Ser.*, vol. 117, edited by S. Karato et al., pp. 133–159, Washington D. C.

Kendall, J.-M., G. W. Stuart, C. J. Ebinger, I. D. Bastow, and D. Keir (2005), Magma-assisted rifting in Ethiopia, *Nature*, *433*(7022), 146–148.

Keranen, K., S. L. Klemperer, R. Gloaguen, and E. W. Group (2004), Three-dimensional seismic imaging of a protoridge axis in the Main Ethiopian rift, *Geology*, *32*(11), 949–952.

Langston, C. A. (1979), Structure under Mount Rainier, Washington, inferred from teleseismic body waves, *J. Geophys. Res.*, *84*, 4749–4762.

Laughton, A. S., and C. Tramontini (1969), Recent studies of the crustal structure in the Gulf of Aden, *Tectonophysics*, *8*, 459–375.

Lemma, Y., A. Hailu, M. Desissa, and U. Kalberkamp (2010), Integrated geophysical surveys to characterize Tendaho geothermal field in north eastern Ethiopia, paper presented at World Geothermal Congress, Indones. Geotherm. Assoc., Bali, Indonesia.

Lithgow-Bertelloni, C., and P. G. Silver (1998), Dynamic topography, plate driving forces and the African superswell, *Nature*, *395*, 269–272.

Lodge, A., and G. Helffrich (2009), Grid-search inversion of teleseismic receiver functions, *Geophys. J. Int.*, *178*, 513–523.

Mackenzie, G. D., H. Thybo, and P. K. H. Maguire (2005), Crustal velocity structure across the Main Ethiopian Rift: results from two-dimensional wide-angle seismic modelling, *Geophys. J. Int.*, *162*(3), 994–1006.

Maguire, P. K. H., et al. (2006), Crustal structure of the northern Main Ethiopian Rift from the EAGLE controlled-source survey: A snapshot of incipient lithospheric break-up, in *The Afar Volcanic Province Within the East African Rift System*, edited by G. Yirgu, C. J. Ebinger, and P. K. H. Maguire, *Geol. Soc. Spec. Publ.*, *259*, 269–292.

Makris, J., and A. Ginzburg (1987), The Afar Depression: Transition between continental rifting and sea-floor spreading, *Tectonophysics*, *141*, 199–214.

Makris, J., H. Menzel, J. Zimmermann, and P. Gouin (1975), Gravity field and crustal structure of northern Ethiopia, in *Afar Depression of Ethiopia: Proceedings of an International Symposium on the Afar Region and Related Rift Problems, Held in Bad Bergzabern, FR Germany, April 1–6, 1974*, pp. 135–144, Schweizerbart, Stuttgart, Germany.

Manighetti, I., P. Tapponnier, V. Courtillot, S. Gruszow, and P. Y. Gillot (1997), Propogation of rifting along the Arabia-

Somalia plate boundary: The gulfs of Aden and Tadjoura, *J. Geophys. Res.*, *102*, 2681–2710.
Manighetti, I., P. Tapponnier, P. Y. Gillot, E. Jacques, V. Courtillot, R. Armijo, J. C. Ruegg, and G. King (1998), Propogation of rifting along the Arabia-Somalia plate boundary: Into Afar, *J. Geophys. Res.*, *103*, 4947–4974.
McClusky, S., R. Reilinger, S. Mahmoud, D. B. Sari, and A. Tealeb (2010), GPS constraints on Africa (Nubia) and Arabia plate motions, *Geophys. J. Int.*, *155*, 126–138.
McKenzie, D. P., and W. J. Morgan (1969), Evolution of triple junctions, *Nature*, *224*, 125–133.
McKenzie, D. P., D. Davies, and P. Molnar (1972), Plate tectonics of the Red Sea and East Africa, *Nature*, *224*, 125–133.
Mechie, J., C. Prodehl, and G. Koptschalitsch (1986), Ray-path interpretation of the crustal structure beneath Saudi Arabia, *Tectonophysics*, *131*, 333–352.
Müller, R. D., C. Gaina, W. R. Roest, and D. L. Hansen (2001), A recipe for microcontinent formation, *Geology*, *29*(3), 203–206.
Park, J., and V. Levin (2000), Receiver functions from multiple-taper spectral correlation estimates, *Bull. Seismol. Soc. Am*, *90*(6), 1507–1520.
Press, W. H., S. A. Teukolsky, W. T. Vetterling, and B. P. Flannery (1992), *Numerical Recipies*, 2nd ed., Cambridge Univ. Press, Cambridge, U. K.
Prodehl, C., and J. Mechie (1991), Crustal thinning in relationship to the evolution of the Afro-Arabian rift system: A revew of seismic-refraction data, *Tectonophysics*, *198*, 311–327.
Prodehl, C., K. Fuchs, and J. Mechie (1997), Seismic-refraction studies of the Afro-Arabian rift system–A brief review, *Tectonophysics*, *278*, 1–13.
Redfield, T., W. Wheeler, and M. Often (2003), A kinematic model for the development of the Afar Depression and its paleogeographic implications, *Earth Planet. Sci. Lett.*, *216*(3), 383–398.
Sebai, A., E. Stutzmann, J. Montagner, D. Sicilia, and E. Beucler (2006), Anisotropic structure of the African upper mantle from Rayleigh and Love wave tomography, *Phys. Earth Planet. Inter.*, *155*(1–2), 48–62.
Siebert, L., and T. Simkin (2002), Volcanoes of the world: an illustrated catalog of holocene volcanoes and their eruptions. smithsonian institution, *Global Volcanism Program Digital Inf. Ser.*, *GVP-3*, Smithsonian Inst., Washington, D. C. [Available at http://www.volcano.si.edu/world/.]
Stuart, G. W., I. D. Bastow, and C. J. Ebinger (2006), Crustal structure of the northern Main Ethiopian Rift from receiver function studies, in *The Afar Volcanic Province Within the East African Rift System*, edited by G. Yirgu, C. J. Ebinger, and P. K. H. Maguire, *Geol. Soc. Spec. Publ.*, *259*, 55–72.
Tesfaye, S., D. J. Harding, and T. M. Kusky (2003), Early continental breakup boundary and migration of the Afar triple junction, Ethiopia, *Geol. Soc. Am. Bull.*, *115*, 1053–1067.
Thompson, D. A., I. D. Bastow, G. Helffrich, J. Kendall, J. Wookey, D. B. Snyder, and D. W. Eaton (2010), Precambrian crustal evolution: Seismic constraints from the canadian shield, *Earth Planet. Sci. Lett.*, *297*, 655–666.
Ukstins, I. A., P. R. Renne, E. Wolfenden, J. Baker, D. Ayalew, and M. Menzies (2002), Matching conjugate volcanic rifted margns: $^{40}Ar/^{39}Ar$ chrono-stratigraphy of pre- and syn-rift bimodal flood volcanism in Ethiopia and Yemen, *Earth Planet. Sci. Lett.*, *198*, 289–306.
Vigny, C., P. Huchon, J.-C. Ruegg, K. Khanbari, and L. M. Asfaw (2006), Confirmation of Arabia plate slow motion by new GPS data in Yemen, *J. Geophys. Res.*, *111*, B02402, doi:10.1029/2004JB003229.
Watanabe, T. (1993), Effects of water and melt on seismic velocities and their application to characterization of seismic reflectors, *Geophys. Res. Lett.*, *20*(24), 2933–2936.
Whaler, K. A., and S. Hautot (2006), The electrical resistivity structure of the crust beneath the northern Main Ethiopian Rift, in *The Afar Volcanic Province Within the East African Rift System*, edited by G. Yirgu, C. J. Ebinger, and P. K. H. Maguire, *Geol. Soc. Spec. Publ.*, *259*, 55–72.
White, R., and D. McKenzie (1989), Magmatism at rift zones: The generation of volcanic continental margins and flood basalts, *J. Geophys. Res.*, *94*, 7685–7729.
WoldeGabriel, G., J. L. Aronson, and R. C. Walter (1990), Geology, geochronology and rift basin development in the central sector of the Main Ethiopian Rift, *Geol. Soc. Am. Bull.*, *102*, 439–458.
Wolfenden, E., C. Ebinger, G. Yirgu, A. Deino, and D. Ayalew (2004), Evolution of the northern Main Ethiopian rift: birth of a triple junction, *Earth Planet. Sci. Lett.*, *224*, 213–228.
Wolfenden, E., C. Ebinger, G. Yirgu, P. R. Renne, and S. P. Kelly (2005), Evolution of a volcanic rifted margin: Southern Red Sea, Ethiopia, *Geol. Soc. Am. Bull.*, *117*, 846–864.
Wright, T., C. Ebinger, J. Biggs, A. Ayele, G. Yirgu, D. Keir, and A. Stork (2006), Magma-maintained rift segmentation at continental rupture in the 2005 Afar dyking episode, *Nature*, *442*(7100), 291–294.
Zandt, G., and C. J. Ammon (1995), Continental crust composition constrained by measurements of crustal Poisson's ratio, *Nature*, *374*, 152–154.
Zhu, L., and H. Kanamori (2000), Moho depth variation in southern California from teleseismic receiver functions, *J. Geophys. Res.*, *105*(B2), 2969–2980.